Search for supersymmetric particles in light gravitino scenarios and sleptons NLSP

J. Abdallah, P. Abreu, W. Adam, P. Adzic, T. Albrecht, T. Alderweireld, R. Alemany-Fernandez, T. Allmendinger, P P. Allport, U. Amaldi, et al.

EUROPEAN ORGANIZATION FOR NUCLEAR RESEARCH

CERN–EP/2002-083

16 October 2002

Search for supersymmetric particles in light gravitino scenarios and sleptons NLSP

DELPHI Collaboration

Abstract

A search for sleptons, neutralinos, charginos, sgoldstinos and heavy stable charged sleptons in the context of scenarios where the lightest supersymmetric particle is the gravitino, is presented. Data collected during 2000 with the DELPHI detector at centre-of-mass energies from 204 to 208 GeV were analysed and combined with all the data collected from 1995 to 1999 at lower energies. No evidence for the production of sleptons, neutralinos and charginos has been found, therefore new limits on the mass of these supersymmetric particles and on the model parameter space are set. The search for heavy stable charged sleptons also updates the stable sleptons mass limit. The absence of evidence for sgoldstino production allows limits to be set on its mass and on the scale of supersymmetry breaking.

(Accepted by Eur. Phys. J. C)

J.Abdallah[24], P.Abreu[22], W.Adam[50], P.Adzic[11], T.Albrecht[17], T.Alderweireld[2], R.Alemany-Fernandez[8], T.Allmendinger[17], P.P.Allport[23], U.Amaldi[28], N.Amapane[44], S.Amato[47], E.Anashkin[35], A.Andreazza[27], S.Andringa[22], N.Anjos[22], P.Antilogus[26], W-D.Apel[17], Y.Arnoud[14], S.Ask[25], B.Asman[43], J.E.Augustin[24], A.Augustinus[8], P.Baillon[8], A.Ballestrero[45], P.Bambade[20], R.Barbier[26], D.Bardin[16], G.Barker[17], A.Baroncelli[38], M.Battaglia[8], M.Baubillier[24], K-H.Becks[52], M.Begalli[6], A.Behrmann[52], E.Ben-Haim[20], N.Benekos[31], A.Benvenuti[5], C.Berat[14], M.Berggren[24], L.Berntzon[43], D.Bertrand[2], M.Besancon[39], N.Besson[39], D.Bloch[9], M.Blom[30], M.Bluj[51], M.Bonesini[28], M.Boonekamp[39], P.S.L.Booth[23], G.Borisov[21], O.Botner[48], B.Bouquet[20], T.J.V.Bowcock[23], I.Boyko[16], M.Bracko[42], R.Brenner[48], E.Brodet[34], P.Bruckman[18], J.M.Brunet[7], L.Bugge[32], P.Buschmann[52], M.Calvi[28], T.Camporesi[8], V.Canale[37], F.Carena[8], N.Castro[22], F.Cavallo[5], M.Chapkin[41], Ph.Charpentier[8], P.Checchia[35], R.Chierici[8], P.Chliapnikov[41], J.Chudoba[8], S.U.Chung[8], K.Cieslik[18], P.Collins[8], R.Contri[13], G.Cosme[20], F.Cossutti[46], M.J.Costa[49], B.Crawley[1], D.Crennell[36], J.Cuevas[33], J.D'Hondt[2], J.Dalmau[43], T.da Silva[47], W.Da Silva[24], G.Della Ricca[46], A.De Angelis[46], W.De Boer[17], C.De Clercq[2], B.De Lotto[46], N.De Maria[44], A.De Min[35], L.de Paula[47], L.Di Ciaccio[37], A.Di Simone[38], K.Doroba[51], J.Drees[52,8], M.Dris[31], G.Eigen[4], T.Ekelof[48], M.Ellert[48], M.Elsing[8], M.C.Espirito Santo[8], G.Fanourakis[11], D.Fassouliotis[11,3], M.Feindt[17], J.Fernandez[40], A.Ferrer[49], F.Ferro[13], U.Flagmeyer[52], H.Foeth[8], E.Fokitis[31], F.Fulda-Quenzer[20], J.Fuster[49], M.Gandelman[47], C.Garcia[49], Ph.Gavillet[8], E.Gazis[31], T.Geralis[11], R.Gokieli[8,51], B.Golob[42], G.Gomez-Ceballos[40], P.Goncalves[22], E.Graziani[38], G.Grosdidier[20], K.Grzelak[51], J.Guy[36], C.Haag[17], A.Hallgren[48], K.Hamacher[52], K.Hamilton[34], J.Hansen[32], S.Haug[32], F.Hauler[17], V.Hedberg[25], M.Hennecke[17], H.Herr[8], J.Hoffman[51], S-O.Holmgren[43], P.J.Holt[8], M.A.Houlden[23], K.Hultqvist[43], J.N.Jackson[23], G.Jarlskog[25], P.Jarry[39], D.Jeans[34], E.K.Johansson[43], P.D.Johansson[43], P.Jonsson[26], C.Joram[8], L.Jungermann[17], F.Kapusta[24], S.Katsanevas[26], E.Katsoufis[31], G.Kernel[42], B.P.Kersevan[8,42], A.Kiiskinen[15], B.T.King[23], N.J.Kjaer[8], P.Kluit[30], P.Kokkinias[11], C.Kourkoumelis[3], O.Kouznetsov[16], Z.Krumstein[16], M.Kucharczyk[18], J.Lamsa[1], G.Leder[50], F.Ledroit[14], L.Leinonen[43], R.Leitner[29], J.Lemonne[2], V.Lepeltier[20], T.Lesiak[18], W.Liebig[52], D.Liko[50], A.Lipniacka[43], J.H.Lopes[47], J.M.Lopez[33], D.Loukas[11], P.Lutz[39], L.Lyons[34], J.MacNaughton[50], A.Malek[52], S.Maltezos[31], F.Mandl[50], J.Marco[40], R.Marco[40], B.Marechal[47], M.Margoni[35], J-C.Marin[8], C.Mariotti[8], A.Markou[11], C.Martinez-Rivero[40], J.Masik[12], N.Mastroyiannopoulos[11], F.Matorras[40], C.Matteuzzi[28], F.Mazzucato[35], M.Mazzucato[35], R.Mc Nulty[23], C.Meroni[27], W.T.Meyer[1], E.Migliore[44], W.Mitaroff[50], U.Mjoernmark[25], T.Moa[43], M.Moch[17], K.Moenig[8,10], R.Monge[13], J.Montenegro[30], D.Moraes[47], S.Moreno[22], P.Morettini[13], U.Mueller[52], K.Muenich[52], M.Mulders[30], L.Mundim[6], W.Murray[36], B.Muryn[19], G.Myatt[34], T.Myklebust[32], M.Nassiakou[11], F.Navarria[5], K.Nawrocki[51], R.Nicolaidou[39], M.Nikolenko[16,9], A.Oblakowska-Mucha[19], V.Obraztsov[41], A.Olshevski[16], A.Onofre[22], R.Orava[15], K.Osterberg[15], A.Ouraou[39], A.Oyanguren[49], M.Paganoni[28], S.Paiano[5], J.P.Palacios[23], H.Palka[18], Th.D.Papadopoulou[31], L.Pape[8], C.Parkes[23], F.Parodi[13], U.Parzefall[8], A.Passeri[38], O.Passon[52], L.Peralta[22], V.Perepelitsa[49], A.Perrotta[5], A.Petrolini[13], J.Piedra[40], L.Pieri[38], F.Pierre[39], M.Pimenta[22], E.Piotto[8], T.Podobnik[42], V.Poireau[39], M.E.Pol[6], G.Polok[18], P.Poropat[†46], V.Pozdniakov[16], N.Pukhaeva[2,16], A.Pullia[28], J.Rames[12], L.Ramler[17], A.Read[32], P.Rebecchi[8], J.Rehn[17], D.Reid[30], R.Reinhardt[52], P.Renton[34], F.Richard[20], J.Ridky[12], M.Rivero[40], D.Rodriguez[40], A.Romero[44], P.Ronchese[35], E.Rosenberg[1], P.Roudeau[20], T.Rovelli[5], V.Ruhlmann-Kleider[39], D.Ryabtchikov[41], A.Sadovsky[16], L.Salmi[15], J.Salt[49], A.Savoy-Navarro[24], U.Schwickerath[8], A.Segar[34], R.Sekulin[36], M.Siebel[52], A.Sisakian[16], G.Smadja[26], O.Smirnova[25], A.Sokolov[41], A.Sopczak[21], R.Sosnowski[51], T.Spassov[8], M.Stanitzki[17], A.Stocchi[20], J.Strauss[50], B.Stugu[4], M.Szczekowski[51], M.Szeptycka[51], T.Szumlak[19], T.Tabarelli[28], A.C.Taffard[23], F.Tegenfeldt[48], J.Timmermans[30], L.Tkatchev[16], M.Tobin[23], S.Todorovova[12], A.Tomaradze[8], B.Tome[22], A.Tonazzo[28], P.Tortosa[49], P.Travnicek[12], D.Treille[8], G.Tristram[7], M.Trochimczuk[51], C.Troncon[27], M-L.Turluer[39], I.A.Tyapkin[16], P.Tyapkin[16], S.Tzamarias[11], V.Uvarov[41], G.Valenti[5], P.Van Dam[30], J.Van Eldik[8], A.Van Lysebetten[2], N.van Remortel[2], I.Van Vulpen[30], G.Vegni[27], F.Veloso[22], W.Venus[36], F.Verbeure[2], P.Verdier[26], V.Verzi[37], D.Vilanova[39], L.Vitale[46], V.Vrba[12], H.Wahlen[52],

A.J.Washbrook[23], C.Weiser[17], D.Wicke[8], J.Wickens[2], G.Wilkinson[34], M.Winter[9], M.Witek[18], G.Wolf[8], O.Yushchenko[41], A.Zalewska[18], P.Zalewski[51], D.Zavrtanik[42], N.I.Zimin[16], A.Zintchenko[16], M.Zupan[11]

[1]Department of Physics and Astronomy, Iowa State University, Ames IA 50011-3160, USA
[2]Physics Department, Universiteit Antwerpen, Universiteitsplein 1, B-2610 Antwerpen, Belgium
and IIHE, ULB-VUB, Pleinlaan 2, B-1050 Brussels, Belgium
and Faculté des Sciences, Univ. de l'Etat Mons, Av. Maistriau 19, B-7000 Mons, Belgium
[3]Physics Laboratory, University of Athens, Solonos Str. 104, GR-10680 Athens, Greece
[4]Department of Physics, University of Bergen, Allégaten 55, NO-5007 Bergen, Norway
[5]Dipartimento di Fisica, Università di Bologna and INFN, Via Irnerio 46, IT-40126 Bologna, Italy
[6]Centro Brasileiro de Pesquisas Físicas, rua Xavier Sigaud 150, BR-22290 Rio de Janeiro, Brazil
and Depto. de Física, Pont. Univ. Católica, C.P. 38071 BR-22453 Rio de Janeiro, Brazil
and Inst. de Física, Univ. Estadual do Rio de Janeiro, rua São Francisco Xavier 524, Rio de Janeiro, Brazil
[7]Collège de France, Lab. de Physique Corpusculaire, IN2P3-CNRS, FR-75231 Paris Cedex 05, France
[8]CERN, CH-1211 Geneva 23, Switzerland
[9]Institut de Recherches Subatomiques, IN2P3 - CNRS/ULP - BP20, FR-67037 Strasbourg Cedex, France
[10]Now at DESY-Zeuthen, Platanenallee 6, D-15735 Zeuthen, Germany
[11]Institute of Nuclear Physics, N.C.S.R. Demokritos, P.O. Box 60228, GR-15310 Athens, Greece
[12]FZU, Inst. of Phys. of the C.A.S. High Energy Physics Division, Na Slovance 2, CZ-180 40, Praha 8, Czech Republic
[13]Dipartimento di Fisica, Università di Genova and INFN, Via Dodecaneso 33, IT-16146 Genova, Italy
[14]Institut des Sciences Nucléaires, IN2P3-CNRS, Université de Grenoble 1, FR-38026 Grenoble Cedex, France
[15]Helsinki Institute of Physics, HIP, P.O. Box 9, FI-00014 Helsinki, Finland
[16]Joint Institute for Nuclear Research, Dubna, Head Post Office, P.O. Box 79, RU-101 000 Moscow, Russian Federation
[17]Institut für Experimentelle Kernphysik, Universität Karlsruhe, Postfach 6980, DE-76128 Karlsruhe, Germany
[18]Institute of Nuclear Physics,Ul. Kawiory 26a, PL-30055 Krakow, Poland
[19]Faculty of Physics and Nuclear Techniques, University of Mining and Metallurgy, PL-30055 Krakow, Poland
[20]Université de Paris-Sud, Lab. de l'Accélérateur Linéaire, IN2P3-CNRS, Bât. 200, FR-91405 Orsay Cedex, France
[21]School of Physics and Chemistry, University of Lancaster, Lancaster LA1 4YB, UK
[22]LIP, IST, FCUL - Av. Elias Garcia, 14-1^{o}, PT-1000 Lisboa Codex, Portugal
[23]Department of Physics, University of Liverpool, P.O. Box 147, Liverpool L69 3BX, UK
[24]LPNHE, IN2P3-CNRS, Univ. Paris VI et VII, Tour 33 (RdC), 4 place Jussieu, FR-75252 Paris Cedex 05, France
[25]Department of Physics, University of Lund, Sölvegatan 14, SE-223 63 Lund, Sweden
[26]Université Claude Bernard de Lyon, IPNL, IN2P3-CNRS, FR-69622 Villeurbanne Cedex, France
[27]Dipartimento di Fisica, Università di Milano and INFN-MILANO, Via Celoria 16, IT-20133 Milan, Italy
[28]Dipartimento di Fisica, Univ. di Milano-Bicocca and INFN-MILANO, Piazza della Scienza 2, IT-20126 Milan, Italy
[29]IPNP of MFF, Charles Univ., Areal MFF, V Holesovickach 2, CZ-180 00, Praha 8, Czech Republic
[30]NIKHEF, Postbus 41882, NL-1009 DB Amsterdam, The Netherlands
[31]National Technical University, Physics Department, Zografou Campus, GR-15773 Athens, Greece
[32]Physics Department, University of Oslo, Blindern, NO-0316 Oslo, Norway
[33]Dpto. Fisica, Univ. Oviedo, Avda. Calvo Sotelo s/n, ES-33007 Oviedo, Spain
[34]Department of Physics, University of Oxford, Keble Road, Oxford OX1 3RH, UK
[35]Dipartimento di Fisica, Università di Padova and INFN, Via Marzolo 8, IT-35131 Padua, Italy
[36]Rutherford Appleton Laboratory, Chilton, Didcot OX11 OQX, UK
[37]Dipartimento di Fisica, Università di Roma II and INFN, Tor Vergata, IT-00173 Rome, Italy
[38]Dipartimento di Fisica, Università di Roma III and INFN, Via della Vasca Navale 84, IT-00146 Rome, Italy
[39]DAPNIA/Service de Physique des Particules, CEA-Saclay, FR-91191 Gif-sur-Yvette Cedex, France
[40]Instituto de Fisica de Cantabria (CSIC-UC), Avda. los Castros s/n, ES-39006 Santander, Spain
[41]Inst. for High Energy Physics, Serpukov P.O. Box 35, Protvino, (Moscow Region), Russian Federation
[42]J. Stefan Institute, Jamova 39, SI-1000 Ljubljana, Slovenia and Laboratory for Astroparticle Physics,
Nova Gorica Polytechnic, Kostanjeviska 16a, SI-5000 Nova Gorica, Slovenia,
and Department of Physics, University of Ljubljana, SI-1000 Ljubljana, Slovenia
[43]Fysikum, Stockholm University, Box 6730, SE-113 85 Stockholm, Sweden
[44]Dipartimento di Fisica Sperimentale, Università di Torino and INFN, Via P. Giuria 1, IT-10125 Turin, Italy
[45]INFN,Sezione di Torino, and Dipartimento di Fisica Teorica, Università di Torino, Via P. Giuria 1,
IT-10125 Turin, Italy
[46]Dipartimento di Fisica, Università di Trieste and INFN, Via A. Valerio 2, IT-34127 Trieste, Italy
and Istituto di Fisica, Università di Udine, IT-33100 Udine, Italy
[47]Univ. Federal do Rio de Janeiro, C.P. 68528 Cidade Univ., Ilha do Fundão BR-21945-970 Rio de Janeiro, Brazil
[48]Department of Radiation Sciences, University of Uppsala, P.O. Box 535, SE-751 21 Uppsala, Sweden
[49]IFIC, Valencia-CSIC, and D.F.A.M.N., U. de Valencia, Avda. Dr. Moliner 50, ES-46100 Burjassot (Valencia), Spain
[50]Institut für Hochenergiephysik, Österr. Akad. d. Wissensch., Nikolsdorfergasse 18, AT-1050 Vienna, Austria
[51]Inst. Nuclear Studies and University of Warsaw, Ul. Hoza 69, PL-00681 Warsaw, Poland
[52]Fachbereich Physik, University of Wuppertal, Postfach 100 127, DE-42097 Wuppertal, Germany
† deceased

1 Introduction

In the year 2000 the Large Electron Positron Collider (LEP) at CERN finished its operation achieving record energies of 204 to 208 GeV when the DELPHI detector collected an integrated luminosity of 223.53 pb^{-1}. These data were analysed to update the searches for sleptons, neutralinos, charginos, sgoldstinos and heavy stable charged particles [1,2] in the context of gauge mediated supersymmetry breaking (GMSB) models.

Supersymmetry (SUSY) is usually assumed to be broken in a hidden sector of particles and then communicated to the observable sector (where all the particles and their superpartners lie) via gravitational interactions. An alternative possibility is that this mediation is performed by Standard Model (SM) gauge interactions, leading to models of gauge mediated supersymmetry breaking. In most current GMSB theoretical work [3–5], it is assumed that the hidden sector is coupled to a messenger sector, which in turn couples to the visible sector through radiative corrections with gauge-interaction strength. The primary motivation for GMSB is that it naturally accommodates the experimentally observed absence of flavour changing neutral currents due to the fact that gauge interactions are flavour blind. In these models the scale of SUSY breaking ($\sqrt{F}$) can be as low as about 10^4 or 10^5 GeV[1] in order to have supersymmetric particle (sparticle) masses of the right order of magnitude (~ 100 GeV/c^2).

The mass of the gravitino ($\tilde{G}$) is related to the scale of SUSY breaking through the expression:

$$m_{\tilde{G}} \simeq 2.5 \times F/(100 \text{ TeV})^2 \text{ eV/c}^2, \tag{1}$$

therefore $m_{\tilde{G}}$ can be as low as few eV/c^2. Consequently in these models $\tilde{G}$ is the lightest supersymmetric particle (LSP) and all the other sparticles will decay into final states that include it. Gravitino masses below $3{\cdot}10^{-4}$ eV/c^2 have been ruled out using Tevatron data for the multijet final states [6]. On the other hand, hints from cosmology point in the direction of either a light gravitino with mass below 1 keV/c^2 or a heavy one with mass above 1 TeV/c^2 [7,10].

In GMSB models the entire minimal supersymmetric standard model (MSSM) spectrum can be predicted in terms of the following parameters:

$$F,\ \Lambda,\ M,\ n,\ \ \tan\beta \text{ and } \mathrm{sign}(\mu). \tag{2}$$

The most important parameter is Λ (the effective SUSY breaking scale) because it sets the overall mass scale of supersymmetric particles. M is the messenger mass scale. The number of messenger generations, n, is also very important because it determines which sparticle is the next-to-lightest supersymmetric particle (NLSP). For $n = 1$ the NLSP is mainly the $\tilde{\chi}_1^0$, and for $n \geq 2$ it is one of the sleptons. The parameter $\tan\beta$ is the ratio of the Higgs vacuum expectation values, and $\mathrm{sign}(\mu)$ is the sign of the Higgs sector mixing parameter[2].

The coupling to the gravitino is very weak, therefore, all the superparticles other than the next-to-lightest supersymmetric particle undergo chain decay down to the NLSP which finally decays to the $\tilde{G}$. The mean decay length ($\hat{L}$) of the NLSP depends on $m_{\tilde{G}}$ [8]. Namely, for $\tilde{l} \to l\tilde{G}$ decay:

$$\hat{L} = 1.76 \times 10^{-3} \sqrt{\left(\frac{E_{\tilde{l}}}{m_{\tilde{l}}}\right)^2 - 1} \left(\frac{m_{\tilde{l}}}{100\,\mathrm{GeV/c^2}}\right)^{-5} \left(\frac{m_{\tilde{G}}}{1\,\mathrm{eV/c^2}}\right)^2 \text{ cm} \tag{3}$$

[1] In gravity mediated SUSY breaking models $\sqrt{F} \sim 10^{10}$ or 10^{11} GeV.

[2] The magnitude of μ is calculable from the other parameters in the model by imposing radiative electroweak symmetry breaking.

where $m_{\tilde{l}}$ is the slepton mass and $E_{\tilde{l}}$ the slepton energy. Therefore, the gravitino mass determines if the NLSP decays inside or outside the detector, giving rise to very interesting topologies explored in this paper. For example, for $m_{\tilde{G}} \lesssim 250$ eV/c^2($\sqrt{F} \lesssim 1000$ TeV), the decay of a NLSP with mass greater than for example 60 GeV/c^2 can take place within the detector. This range of $\sqrt{F}$ is in fact consistent with astrophysical and cosmological considerations [9,10]. Figure 1 shows the $\tilde{\tau}$ mean decay length as a function of the gravitino mass for different $\tilde{\tau}$ masses.

In this paper data were analysed within the two possible slepton NLSP scenarios as discussed in the following. Depending on the magnitude of the mixing in the third family between the left and right gauge eigenstates, $\tilde{\tau}_R$ and $\tilde{\tau}_L$, there are two possible scenarios. If the mixing is large[3], $\tilde{\tau}_1$ (the lighter mass eigenstate) is the NLSP. However, if the mixing is negligible, $\tilde{\tau}_1$ is mainly right-handed [11] and almost mass degenerate with the other sleptons. In this case, the $\tilde{e}_R$ and $\tilde{\mu}_R$ three body decay ($\tilde{l} \rightarrow \tilde{\tau}_1 \tau l$ with $\tilde{\tau}_1 \rightarrow \tau \tilde{G}$), is very suppressed, and $\tilde{e}_R$ and $\tilde{\mu}_R$ decay directly into $l\tilde{G}$. This scenario is called sleptons co-NLSP.

The signature for SUSY particle production within GMSB models at LEP2 depends on the NLSP type and on its mean decay length, or equivalently, on the gravitino mass. The NLSP could be pair produced directly, or other sparticle production could lead to a cascade decay into the NLSP. The NLSP will decay into its non-SUSY partner and a $\tilde{G}$. Taking into account all these factors, the following topologies can be expected:

- For $m_{\tilde{G}}$ below a few eV/c^2, the NLSP decays in the vicinity of its production point, before the tracking devices of the detector, and different topologies can be expected. If the sleptons are pair produced the signature in the detector is the same as in the search for sleptons in gravity-mediated supersymmetry breaking scenarios (MSUGRA) with $\tilde{\chi}_1^0$ LSP, i.e. two acoplanar[4] leptons and missing energy [12] since the slepton decays into a lepton and a neutralino that escapes detection. This process is topologically equivalent to the pair production of two sleptons and each of them decaying into a lepton and a gravitino (if $m_{\tilde{G}}$ is below a few eV/c^2). However, if neutralino pair production is kinematically allowed, the production cross-section can be larger than for $\tilde{l}$ even if $m_{\tilde{\chi}_1^0} > m_{\tilde{l}}$ because of the β^3 suppression factor of the scalar production cross-section. In this case the topology is given by four leptons and missing energy since each $\tilde{\chi}_1^0$ decays into $\tilde{l}l$, and the sleptons into $l\tilde{G}$. The mass region that can be inspected using this search can be complemented with the search for lightest neutralino pair production when the neutralino is the NLSP decaying into a photon and a gravitino [13].
- For $m_{\tilde{G}}$ between a few eV/c^2 and a few hundred eV/c^2 the NLSP has an intermediate mean decay length and it would decay in flight in some part of the detector volume. This creates well defined secondary vertices or kinks when the $\tilde{l}$ is reconstructed by the tracking devices, or large impact parameter tracks if it is not.
- For gravitino masses above few hundred eV/c^2 the NLSP would be sufficiently long-lived to decay outside the detector giving rise to heavy stable charged particle signatures.

In the GMSB parameter space where the $\tilde{\chi}_1^0$ is the NLSP, the chargino is always much heavier than 100 GeV/c^2 [14] and, therefore, cannot be produced at LEP. On the contrary, in the parameter space where the $\tilde{l}$ is the NLSP there are regions where the $\tilde{\chi}_1^{\pm}$ is light enough to be produced [15]. In this case the topology for $m_{\tilde{G}}$ below a few eV/c^2 is again

[3] In GMSB models large mixing occurs generally in regions of $\tan\beta \geq 10$ or $|\mu| > 500$ GeV/c^2.

[4] Acoplanarity is defined as the complement of the angle between the projections of the two tracks onto the plane perpendicular to the beam.

two acoplanar leptons and missing energy since each $\tilde{\chi}_1^{\pm}$ decays into $\tilde{l}\nu$ and each $\tilde{l}$ into $l\tilde{G}$. For $m_{\tilde{G}}$ between a few eV/c^2 and a few hundred eV/c^2 the topologies are kinks or large impact parameter tracks and, for gravitino masses above a few hundred eV/c^2, heavy stable charged particle signatures are expected.

In this paper, the update of the search for heavy stable charged particles is also performed. This kind of particle is predicted not only in GMSB models but also in MSSM with a very small amount of R-parity violation [16], or with R-parity conservation if the mass difference between the LSP and the NLSP becomes very small (references in [17]). The typical signature of these events is two massive particles traversing the detector which do not produce Cherenkov radiation in DELPHI's Ring Imaging CHerenkov (RICH) detectors, but high ionization losses in the Time Projection Chamber. Updated lower mass limits on heavy stable charged particles, under the assumption that the LSP is a charged slepton, are presented.

Recently it has been pointed out [18] that an appropriate theory must also contain the supersymmetric partner of the goldstino, called the sgoldstino, which could be massive. In the minimal R-parity conserving model, as considered in [18], the effective theory at the weak scale contains two neutral scalar states: S, CP-even and P, CP-odd (from now on the two states will be labelled with the generic symbol ϕ since the discussion applies to both of them). It must be pointed out that sgoldstinos have even R-parity, therefore they are not necessarily produced in pairs and their decay chains do not necessarily contain the LSP. The production of these supersymmetric particles may be relevant at LEP2 energies in light gravitino scenarios. One of the most interesting production channels is the process $e^+e^- \to \phi\gamma$ which depends on the ϕ mass (m_ϕ) and on $\sqrt{F}$. The most relevant ϕ decay modes are $\phi \to \gamma\gamma$ and $\phi \to gg$. The corresponding branching ratios depend on the gaugino masses M_1, M_2 and M_3, and the total width is $\Gamma \sim \Gamma(\phi \to \gamma\gamma) + \Gamma(\phi \to gg)$. In this paper two sets for these parameters are considered as suggested in [18]; they are listed in Table 1. The total width for a large interval of the parameter space is narrow (below a few GeV/c^2), except for the region with small $\sqrt{F}$ where the production cross-section is expected to be very large. The two decay channels considered produce events with very different topologies. The channel $\phi \to \gamma\gamma$ gives events with three high energetic photons, one of which has monochromatic energy ($E_\gamma = \frac{s-m_\phi^2}{2\sqrt{s}}$) for a large fraction of the parameter space where ϕ has a negligible width. Despite the lower ϕ decay branching ratio (4 and 11% for the two sets of Table 1, respectively), this final state is worth investigating because the main background source is the QED process $e^+e^- \to \gamma\gamma(\gamma)$, which is expected to be small if photons in the forward region are discarded. On the other hand, the channel $S \to gg$ gives events with one monochromatic photon (except for the region with small $\sqrt{F}$) and two jets. An irreducible background from $e^+e^- \to q\bar{q}\gamma$ events is associated to this topology and therefore the signal must be searched for as an excess of events over the background expectations for every mass hypothesis.

	M_1	M_2	M_3	$BR(\phi \to \gamma\gamma)$	$BR(\phi \to gg)$
1)	200	300	400	4%	96%
2)	350	350	350	11%	89%

Table 1: Two choices for the gaugino mass parameters (in GeV/c^2) relevant for the sgoldstino production and decay, and the corresponding branching ratios (BR) of the two channels considered. The BR are almost independent of m_ϕ in the mass region below 200 GeV/c^2.

The list of GMSB signatures analysed in this paper is given in Table 2.

Production	Decay mode	$\hat{L}$	Expected topology
$e^+e^- \to \tilde{l}\tilde{l}$	$\tilde{l} \to l\tilde{G}$	$<< \ell_{detector}$ $\sim \ell_{detector}$ $>> \ell_{detector}$	Acoplanar leptons Kinks and large impact parameters Heavy stable charged particles
$e^+e^- \to \tilde{\chi}_1^0\tilde{\chi}_1^0$	$\tilde{\chi}_1^0 \to \tilde{l}l \to ll\tilde{G}$	$<< \ell_{detector}$	Four leptons
$e^+e^- \to \tilde{\chi}_1^+\tilde{\chi}_1^-$	$\tilde{\chi}_1^+ \to \tilde{l}^+\nu \to l^+\tilde{G}\nu$	$<< \ell_{detector}$ $\sim \ell_{detector}$ $>> \ell_{detector}$	Acoplanar leptons Kinks and large impact parameters Heavy stable charged particles
$e^+e^- \to \phi\gamma$	$\phi \to \gamma\gamma$ $\phi \to gg$	$<< \ell_{detector}$ $<< \ell_{detector}$	3 high energetic γ 1 monochromatic γ and 2 jets

Table 2: Final state topologies studied in the different scenarios.

The organization of the paper is as follows. A brief description of the DELPHI detector is presented in section 2. The data samples are described in section 3. The different selection criteria, the efficiencies and the number of events selected in data and in the expected Standard Model background are reported in section 4. Finally, the results are presented in section 5 comprising cross-section limits of the pair produced sparticles, lower mass limits and limits on the GMSB model parameters.

2 Detector description

DELPHI was one of the four detectors operating at the LEP collider from 1989 to 2000. It was designed as a general purpose detector for e^+e^- physics with special emphasis on precise tracking and vertex determination and on powerful particle identification. A detailed description of the DELPHI detector can be found in [19] and the detector and trigger performance in [20,21]. Here only those components relevant for the present analyses are discussed.

Charged particle tracks are reconstructed by a system of tracking chambers inside the 1.2 T solenoidal magnetic field: the Vertex Detector (VD), the Inner Detector (ID), the Time Projection Chamber (TPC) and the Outer Detector (OD) in the barrel region; two sets of planar drift chambers aligned perpendicular to the beam axis (Forward Chambers A and B) measure tracks in the forward and backward directions.

For the data presented here, the VD consists of three cylindrical layers of silicon detectors, at radii 6.3 cm, 9.0 cm and 11.0 cm, and polar angle acceptance from 24° to 156°. All three layers measure coordinates in the plane transverse to the beam (xy), and at least two of the layers also measure z coordinates along the beam direction. The ID consists of a cylindrical drift chamber with inner radius 12 cm and outer radius 22 cm, surrounded by 5 layers of straw tubes, having a polar acceptance between 15° and 165°. The TPC, the principal tracking device of DELPHI, consists of a 2.7 m long cylinder of 30 cm inner radius and 122 cm outer radius. Each end-plate of the TPC is divided into 6 sectors with 192 sense wires and 16 circular pad rows per sector. The wires help in charged particle identification by measuring the specific energy loss (dE/dx) and the pad rows are used for 3 dimensional space-point reconstruction. The OD consists of 5 layers

of drift cells at radii between 192 cm and 208 cm, covering polar angles between 43° and 137°.

The electromagnetic calorimeters consist of a High Density Projection Chamber (HPC) covering the polar angle region from 40° to 140° and, a Forward ElectroMagnetic Calorimeter (FEMC) covering the polar angle regions from 11° to 36° and from 144° to 169°. The Scintillator TIle Calorimeter (STIC) extends the polar angle coverage down to 1.66° from the beam axis in both directions. The Hadron CALorimeter (HCAL) covers 98% of the solid angle. The muons which traverse the HCAL are recorded in a set of Muon Drift Chambers placed in the barrel, forward and backward regions.

The Ring Imaging CHerenkov (RICH) detectors of DELPHI provide charged particle identification in both the barrel (BRICH) and forward (FRICH) regions. They contain two radiators of different refractive indices. The liquid radiator is used for particle identification in the momentum range from 0.7 to 8 GeV/c. The gas radiator is used for particles with momentum range from 2.5 GeV/c to 25 GeV/c.

3 Data sample and event generators

The searches reported in this paper are based on data collected with the DELPHI detector during 2000 at centre-of-mass energies from around 204 to 208 GeV. The total integrated luminosity was 223.53 pb^{-1}. Table 3 summarises the energies analysed and the integrated luminosities corresponding to each energy during the LEP2 period.

Year	1995	1996	1997	1998	1999	2000
$\sqrt{s}$ (GeV)	130-136	161-172	183	189	192-202	204-208
$\mathcal{L}$ (pb^{-1})	11.9	19.6	54.0	158.0	228.2	223.5

Table 3: Centre-of-mass energies analysed and their corresponding integrated luminosities during the LEP2 period.

To evaluate the signal efficiencies and background contamination, events were generated using different programs, all relying on `JETSET` 7.4 [22], tuned to LEP1 data [23] for quark fragmentation.

Slepton pair samples at 208 GeV centre-of-mass energy were produced with `PYTHIA` 5.7 [22] with sleptons having mean decay lengths from 0.25 to 200 cm and masses from 60 to 104 $\mathrm{GeV/c^2}$. Other samples of slepton pairs were produced at 206 and 208 GeV with `SUSYGEN` [24] for the small impact parameter search with $m_{\tilde{\tau}}$ from 90 $\mathrm{GeV/c^2}$ to 102 $\mathrm{GeV/c^2}$ and $m_{\tilde{\mu}}$ equal to 90 $\mathrm{GeV/c^2}$. A sample of selectrons with mass equal to 90 $\mathrm{GeV/c^2}$ was produced at 206 GeV. Neutralino pair events and their subsequent decay products were generated with `SUSYGEN`. Selection efficiencies were computed from samples with neutralino masses from 72 $\mathrm{GeV/c^2} \leq m_{\tilde{l}} + 2\ \mathrm{GeV/c^2} \leq m_{\tilde{\chi}_1^0} \leq \sqrt{s}/2$ at 206 GeV. `SUSYGEN` was also used to generate the chargino pair production and decay. In order to compute detection efficiencies, samples at 204 GeV and 206 GeV centre-of-mass energies were generated with gravitino masses of 1, 100 and 1000 $\mathrm{eV/c^2}$, $m_{\tilde{l}} + 0.3\ \mathrm{GeV/c^2} \leq m_{\tilde{\chi}_1^+} \leq \sqrt{s}/2$ and $80\ \mathrm{GeV/c^2} \leq m_{\tilde{l}} \leq \sqrt{s}/2 - 2.6\ \mathrm{GeV/c^2}$. Samples with smaller $\Delta m = m_{\tilde{\chi}_1^+} - m_{\tilde{\tau}_1}$ were not generated because in that region each chargino decays into a W and a gravitino with an appreciable branching ratio.

In the search for heavy stable charged particles, signal efficiencies were estimated from pair produced heavy smuons generated at energies of 205 GeV, 206.7 GeV and 208 GeV

with SUSYGEN. The events were passed through the detector simulation as heavy muons. The efficiencies were estimated for masses between 10 GeV/c^2 and 100 GeV/c^2.

For the sgoldstino search, signal efficiencies for the channel $\phi \rightarrow \gamma\gamma$ were estimated from QED background events generated according to [25]. On the other hand, the selection efficiency for the $\phi \rightarrow gg$ channel was evaluated using $q\overline{q}\gamma$ background events generated with PYTHIA and processed through the full DELPHI analysis chain and reweighted according to the background and signal photon polar angle distribution.

The background process $e^+e^- \rightarrow q\bar{q}(n\gamma)$ was generated with PYTHIA 6.125, while KORALZ 4.2 [26] was used for $\mu^+\mu^-(\gamma)$ and $\tau^+\tau^-(\gamma)$. The generator BHWIDE [27] was used for $e^+e^- \rightarrow e^+e^-$ events. Processes leading to four-fermion final states were generated using EXCALIBUR 1.08 [28] and GRC4F [29]. Two-photon interactions leading to hadronic final states were generated using TWOGAM [30], including the VDM, QPM and QCD components. The generators of Berends, Daverveldt and Kleiss [31] were used for the leptonic final states.

The cosmic radiation background was studied using cosmic muons collected before the beginning of the 2000 LEP run.

The generated signal and background events were passed through the detailed simulation [20] of the DELPHI detector and then processed with the same reconstruction and analysis programs used for real data.

4 Data selection

The following sections describe the selection criteria used to search for the different topologies summarized in Table 2. The searches for slepton, neutralino and chargino pair production are based on the ones described in [1,32–35]. The search for heavy stable charged sleptons is based on the analysis already published in [1,36,37]. Finally the sgoldstino search has already been presented in [2].

4.1 Slepton pair production

This section describes the selection criteria used in the search for the process $e^+e^- \rightarrow \tilde{l}^+\tilde{l}^- \rightarrow l^+\tilde{G}l^-\tilde{G}$. Loose preselection cuts were imposed on the events in order to suppress as much as possible the low energy background (beam-gas and beam-wall) and the SM processes. The reconstructed tracks of charged particles were required to satisfy certain quality criteria: momenta above 100 MeV/c and impact parameters (geometric signed) below 4 cm in the plane transverse to the beam pipe (xy), and below 10 cm in the direction along the beam pipe (z). Clusters in the calorimeters were interpreted as neutral particles if they were not associated to charged particles and if their energy exceeded 100 MeV. Only these particles were used to compute the general event quantities. The preselection cuts were the following:

- to eliminate high multiplicity events like $e^+e^- \rightarrow q\overline{q}(n\gamma)$ or WW, W$e\nu_e$ and ZZ when the produced particles had pure hadronic or semileptonic decays, the multiplicity computed with the particles that satisfied the quality requirements was required to be between 1 and 6 (the multiplicity of all signal samples was very well contained between these two limits);
- to eliminate two-photon processes, the visible energy in the event was required to be above 10 GeV;

- to eliminate the remaining contribution of two-photon and two-fermion processes, the absolute value of the transverse momentum vector of charged and neutral particles was required to be greater than 5 GeV/c;
- the energy measured in the very forward calorimeters (STIC) was required to be below 10 GeV to eliminate the residual contamination of processes mentioned above;
- to eliminate the Bhabha contribution, the total electromagnetic energy was required to be less than the beam energy.

All the events that survive the preselection cuts underwent the search for secondary vertices or kinks. Only the events which were not tagged as kink candidates passed the selection criteria to search for large impact parameter tracks.

4.1.1 Search for secondary vertices or kinks

The analysis exploits a peculiarity of the $\tilde{l}^{\pm} \rightarrow l^{\pm}\tilde{G}$ topology in the case of intermediate gravitino masses (i.e. few eV/c^2< $m_{\tilde{G}}$ < few hundred eV/c^2), namely, one or two tracks coming from the interaction point and at least one of them with either a secondary vertex or a kink.

All the charged particles of the event that survived the preselection cuts were grouped into clusters (in order to group all the particles coming from a tau decay) according to their first measured point in the xy plane. This clustering procedure was iterative and worked as follows. The pair of particles with the smallest separation at their respective starting points was considered first. If this separation was smaller than 2 cm, the particles were grouped to form a cluster whose starting point was defined as the average of their first measured points. The two particles were then replaced by this cluster which was subsequently treated as a pseudo-particle. The process was then repeated until all charged particles or pseudo-particles were grouped into clusters. This procedure allowed for clusters containing a single particle if its momentum was larger than 1.5 GeV/c. Events were rejected if more than 6 particles were not grouped into clusters or if a cluster could not be obtained. This cut was intended to eliminate the remaining beam related background events[5] that had not been excluded at the preselection level.

Once all the particles were grouped in clusters, the search for kinks was performed in the following way. Slepton candidates were searched for among all the clusters in the event. Among the remaining clusters, the ones corresponding to lepton candidates or decay products of taus were also searched for. The clusters were extrapolated in order to find a crossing point. If the crossing point existed, the event was considered as a kink candidate. Reconstruction of secondary vertices for the case $\tilde{\tau} \rightarrow \tau\tilde{G}$ is illustrated in Figure 2, which shows a decay vertex and the variables used in the analysis.

Isolated particles (clusters with only one particle) were considered as $\tilde{l}$ candidates if their trajectories were compatible with particles coming from the interaction point according to the following selection criteria:

- the first measured point with respect to the beam spot in the plane transverse to the beam axis ($R^{\tilde{l}}_{sp}$) had to lie in the Vertex Detector (VD);
- the momentum of the particle was greater than 2 GeV/c;
- the polar angle with respect to the beam axis had to satisfy $|\cos\theta| < 0.8$, corresponding to the barrel region;
- the impact parameter along the beam axis and in the plane perpendicular to it was less than 10 and 4 cm, respectively.

[5]This kind of event was mainly characterized by a high number of low momentum charged particles seen only in the innermost detectors VD and ID.

For every $\tilde{l}$ candidate, a search was made for a second cluster satisfying the following selection criteria:

- the starting point in the transverse plane ($R^{l_d}_{sp}$) had to be greater than $R^{\tilde{l}}_{sp}$. The second cluster starting point was always found in the Inner Detector (ID) or the Time Projection Chamber (TPC);
- the angular separation between the directions defined by the $\tilde{l}$ candidate and the lepton candidate had to be smaller than 45° in the xy plane, to consider only the particles which were in the direction of the slepton.

The $\tilde{l}$ candidate and the lepton cluster had to define a common crossing point, called secondary vertex or kink. If the lepton cluster included more than one charged particle (which is the case when l is a τ decaying to 3 or 5 prongs), only the one with the highest momentum was used to search for the kink. To find the crossing point, the particle trajectories were represented by a helix in space. Taking into account this parametrization, the point of closest approach between the $\tilde{l}$ particle and the selected particle from the l_d cluster was calculated. The conditions to define a good crossing point between both particles were the following:

- the minimum distance between the particles had to be smaller than 1 mm in the xy plane;
- the crossing point, the end point of the slepton and the starting point of the lepton were required to satisfy the following conditions:

$$\begin{aligned} -10\,\mathrm{cm} &< (R_{cross} - R^{\tilde{l}}_{end}) < 25\,\mathrm{cm} \\ -25\,\mathrm{cm} &< (R_{cross} - R^{l}_{sp}) < 10\,\mathrm{cm}, \end{aligned} \tag{4}$$

  where $R^{\tilde{l}}_{end}$, R_{cross} and R^{l}_{sp} are the distances w.r.t the beam spot of the end point of the slepton, the crossing point and the starting point of the lepton in the xy plane. The cut was optimised to assure that all VD or IDVD only particles (particles which only had ID or VD hits) were connected with particles reconstructed with the TPC.

The resolution achieved (generated distance minus reconstructed distance) with the algorithm to find secondary vertices in the coordinates x and y was 0.14 mm. The z coordinate was not taken into account in the search for a crossing point because the resolution for low momentum particles is very poor.

Fake decay vertices could be present among the reconstructed secondary vertices. They could be produced by particles interacting in the detector material or by radiated photons when the particle trajectory was reconstructed as two separated particles. To eliminate these events, additional conditions were required:

- to reject hadronic interactions, the angle between the direction of any reconstructed hadronic vertex w.r.t. beam spot (secondary vertices reconstructed in region where there is material) and the direction of the slepton candidate must be greater than 5°;
- to reject segmented tracks, the angle between the particles used to define a vertex had to be larger than 6°;
- to reject photon radiation in the case of l clusters with only one particle, there had to be no neutral particle in a 3° cone around the direction defined by the difference between the $\tilde{l}$ momentum and the momentum of the l calculated at the crossing point.

If no pair of particles was found to survive these conditions, the event was rejected. Figure 3 shows the distribution of these three quantities. The distributions compare real data, expected SM background simulation and a simulated signal for $m_{\tilde{\tau}}$= 60 GeV/c^2 with a mean decay length of 50 cm.

Table 4 shows the different SM background contributions and the observed events in data after applying the selection criteria to search for kinks. Efficiencies for different gravitino and stau masses were calculated by applying the above selections to the simulated signal samples. Figure 4 shows the secondary vertex reconstruction efficiency as a function of the stau decay radius. For smuons and selectrons the same dependence is observed. For smuons the efficiency plateau is around 60%, while for selectrons it is around 40% due to the preselection cut on total electromagnetic energy.

Observed events	2
Total background	$0.88^{+1.35}_{-0.15}$
$Z^*/\gamma \to (\tau\tau)(n\gamma)$	$0.16^{+0.09}_{-0.05}$
$Z^*/\gamma \to (ee)(n\gamma)$	$0.00^{+0.87}_{-0.00}$
4-fermion (except $\gamma\gamma$)	$0.12^{+0.06}_{-0.01}$
$\gamma\gamma \to \tau^+\tau^-$	$0.16^{+0.32}_{-0.06}$
$\gamma\gamma \to e^+e^-$	$0.44^{+0.98}_{-0.11}$

Table 4: Number of observed events at $\sqrt{s}$ from 204 GeV to 208 GeV together with the total number of expected SM background events and the expected numbers from the individual background sources, for the secondary vertex search. The asymmetric errors are due to the Poissonian description of the statistics.

4.1.2 Large impact parameter search

To investigate the region of low gravitino masses (short decay lengths) the previous search was extended to the case of sleptons decaying between 0.25 cm and around 10 cm, i.e., before the tracking devices. In this case it was only possible to reconstruct the slepton decay products. The impact parameter search was only applied to those events accepted by the same preselection cuts as in the search for secondary vertices but not selected by the vertex analysis. The events used in this search contained exactly two single particle clusters (i.e. two charged particles with momentum larger than 1.5 GeV/c and a distance between starting points greater than 2 cm) which were acollinear and had large impact parameters. The events were accepted as candidates if:

- the first measured point in the xy plane of at least one of the particles was in the VD;
- both particles were reconstructed with the TPC to guarantee good particle reconstruction quality;
- at least one of the particles had an impact parameter w.r.t. the beam spot larger than 0.2 cm in the xy plane to remove SM events;
- the ratio of the maximum impact parameter over the minimum impact parameter in the xy plane and w.r.t. the beam spot was smaller than -1.5 or larger than -0.5, to reject cosmic rays since they are characterized by large impact parameters of the same value and opposite sign.

- the acollinearity[6] between the two particles was larger than 10° to eliminate back-to-back events with badly reconstructed particles or interactions which always gave small acollinearities. In addition, to reduce further the cosmic ray background, the acollinearity between the two particles was required to be smaller than 175°, since an off-time cosmic ray crossing from one TPC drift half to the other could be reconstructed as two almost parallel particles.

Figure 5 shows the acollinearity distribution for real data minus simulated SM background, compared to cosmic rays for events which passed the preselection cuts and cuts 1-3. The latter follows pretty well the acollinearity distribution of the former difference.

Table 5 shows the different SM background contributions and the number of events observed in data after applying the selection criteria to search for large impact parameter particles.

Observed events	2
Total background	$2.40^{+1.44}_{-0.36}$
$Z^*/\gamma \to (\tau\tau)(n\gamma)$	$0.05^{+0.05}_{-0.01}$
$Z^*/\gamma \to (ee)(n\gamma)$	$0.12^{+0.90}_{-0.10}$
4-fermion (except $\gamma\gamma$)	$0.65^{+0.09}_{-0.05}$
$\gamma\gamma \to \tau^+\tau^-$	$0.09^{+0.31}_{-0.04}$
$\gamma\gamma \to e^+e^-$	$1.49^{+1.08}_{-0.34}$

Table 5: Number of observed events at $\sqrt{s}$ from 204 GeV to 208 GeV together with the total number of expected SM background events and the expected numbers from the individual background sources, for the large impact parameter track search. The asymmetric errors are due to the Poissonian description of the statistics.

The efficiencies were derived for different slepton masses and decay lengths by applying the same selection criteria to the simulated signal events. In the search for $\tilde{\tau}_1$ the maximum efficiency was around 32% corresponding to a mean decay length of 2.5 cm. The efficiency decreased sharply for lower decay lengths due to the requirement on minimum impact parameter. For longer decay lengths, the appearance of reconstructed $\tilde{l}$ in combination with the cut on the maximum number of charged particles in the event caused the efficiency to decrease smoothly. This decrease was compensated by a rising efficiency in the search for secondary vertices. For masses above 60 GeV/c^2 no dependence on the $\tilde{l}$ mass was found far from the kinematic limit.

The same selection was applied to smuons and selectrons. For smuons the efficiency increased to $\sim 58\%$ for a mean decay length of 2.5 cm and masses over 60 GeV/c^2 since the smuon always had a one-prong decay. For selectrons the efficiency was $\sim 33\%$ for the same mean decay length and range of masses.

4.1.3 Small impact parameter search

The large impact parameter search can be extended further to mean decay lengths below 0.1 cm. Charged particles were selected if their impact parameter was less than 10 cm in the plane transverse to the beam direction and less than 15 cm in the direction along the beam pipe. The polar angle had to be between 20° and 160°. Their measured

[6]The acollinearity is defined as being 180° minus the angle between the momentum vectors of both particles.

momentum was required to be larger than 400 MeV/c with relative error less than 100% and track length larger than 30 cm. Any calorimetric deposit associated to a discarded charged particle was assumed to come from a neutral particle.

The search was restricted to events with 2 to 4 charged particles and missing energy larger than $0.3\sqrt{s}$. The $\gamma\gamma$ events were suppressed by requiring a visible energy greater than $0.08\sqrt{s}$ and a transverse missing momentum greater than $0.03\sqrt{s}$. The polar angle of the missing momentum was required to be between 30° and 150°, and the total energy in a cone of 30°, E_{30}, around the beam-pipe was required to be less than 10% of the visible energy, and the neutral energy was required to be less than $0.175\sqrt{s}$.

The events were then divided into two hemispheres using the thrust axis. The total momentum of charged and neutral particles in each hemisphere was computed and used to define the acollinearity of the event. Standard $e^+e^- \rightarrow f\overline{f}(\gamma)$ processes and cosmic rays were reduced by requiring the acollinearity to be greater than 10°. The charged particle with the largest and good quality momentum ($\Delta p_i/p_i < 50\%$) in each hemisphere was selected as the leading particle. The following quality requirements were only applied to the leading particles: the first measured point of the particle tracks had to be within 50 cm of the beam spot in the xy plane, the particles were required to have at least one segment beyond the ID detector and to be away from insensitive regions of the electromagnetic calorimeter. In addition, at least one of the leading particles was required to be reconstructed with the TPC.

$e^+e^- \rightarrow f\overline{f}(\gamma)$ processes and cosmic rays were further reduced by requiring an angle between the leading particles in the xy plane of less than 3 radians. Hadronic events, in particular $\gamma\gamma \rightarrow q\overline{q}$ or, in general, events where the available energy is shared by many particles (including undetected/unselected), were rejected by requiring $\sqrt{p_1^2 + p_2^2} > 0.03\sqrt{s}$, where p_1 and p_2 are the momenta of the leading particles. To reduce Bhabha events the total electromagnetic energy of the leading particles, $E_1 + E_2$, had to be less than $0.35\sqrt{s}$. By requiring that any leading particle with an impact parameter larger than 1 cm in the xy plane and measured w.r.t. the beam spot should be reconstructed by the TPC and at least one other detector, the residual cosmic rays (in particular the out-of-time cosmic rays) were rejected. Finally, photon conversion events with only two particles were rejected by requiring the angle between them at their perigee to be greater than 5°.

The background left after the selection described above consisted mainly of events containing τ pairs in the final state ($\gamma^*/Z^* \rightarrow \tau\tau$ and WW $\rightarrow \tau\nu\tau\nu$). To reject these events, the variable $\sqrt{b_1^2 + b_2^2}$, where b_1 and b_2 are the impact parameters in xy (measured w.r.t. the beam spot) of the two leading particles, was used. Requiring $\sqrt{b_1^2 + b_2^2} \geq 0.06$ cm eliminated most of the remaining background.

In order to preserve the efficiency in the region of decay length above 10 cm, where the $\tilde{l}$ can be observed as a particle coming from the primary vertex and badly measured due to its limited length, further requirements on the particle quality were applied only to the leading particle with the largest impact parameter (measured w.r.t. the beam spot). This particle was required to have a relative momentum error < 30% and the particle had to be measured at least either in the TPC or in all of the other three tracking detectors in the barrel (VD, ID and OD).

The efficiency of the search did not show any significant dependence on the $\tilde{l}$ mass for masses over 40 GeV/c^2 and far from the kinematic limit, and it could be parameterized as a function of the $\tilde{l}$ decay length in the laboratory system. The efficiency for $\tilde{\tau}_1$ detection reaches $\sim$ 40% for decay lengths around 2 cm. It is still 16% for a decay length of 0.1 cm,

and 13% for 20 cm. The efficiency for $\tilde{\mu}$ detection reaches 45% around 2 cm, 15% at 0.1 cm, and 17% at 20 cm.

In order to increase the efficiency in the search for selectrons, the cut $(E_1 + E_2) < 0.35\sqrt{s}$ was not applied. The Bhabha events that survived the selection were those where at least one of the electrons underwent a secondary interaction, thus acquiring a large impact parameter. However, it was found that in these cases the measured momentum of the electron was smaller than the electromagnetic energy deposition around the electron track. Therefore, the cut $(E_1/p_1 + E_2/p_2) < 2.2$ was used for the selectron search. The maximum efficiency reached in the selectron search was $\sim 35\%$ at ~ 2 cm mean decay length.

The number of events selected in the data was 4 in the $\tilde{\tau}$ and $\tilde{\mu}$ search. The same 4 events also passed the $\tilde{e}$ search. The expected SM background in both searches was 3.3±0.3 events. Figure 6 shows the $\sqrt{b_1^2 + b_2^2}$ distribution for data (dots), simulated SM backgrounds (grey histogram) and simulated signal of $m_{\tilde{\tau}_1} = 90$ GeV/c^2 and $m_{\tilde{G}} = 25$ eV/c^2 at $\sqrt{s} = 206$ GeV and a boosted mean decay length of around 1 cm (white histogram) after all other cuts. This figure only shows two of the candidates. The other two events not shown have $\sqrt{b_1^2 + b_2^2} \sim 1.5$ cm. The overflow bin has 1.3 expected events from Monte Carlo and 2 from data. All the selected candidates were compatible with SM events.

4.2 Neutralino pair production

In this section, the selections used to search for the process $e^+e^- \to \tilde{\chi}_1^0\tilde{\chi}_1^0 \to \tilde{\tau}_1\tau\tilde{\tau}_1\tau \to \tau\tilde{G}\tau\tau\tilde{G}\tau$ within the $\tilde{\tau}_1$ NLSP scenario, and the process $e^+e^- \to \tilde{\chi}_1^0\tilde{\chi}_1^0 \to \tilde{l}l\tilde{l}'l' \to l\tilde{G}ll'\tilde{G}l'$ (with BR$(\tilde{\chi}_1^0 \to \tilde{l}l) = 1/3$ for each leptonic flavour) within the co-NLSP scenario, are presented.

In the following, the preselection of the events, common to both scenarios, is presented. The reconstructed tracks of charged particles were required to have momenta above 100 MeV/c and impact parameters below 4 cm in the transverse plane and below 10 cm in the longitudinal direction. The relative error on the measurement of the momentum had to be smaller than 100%. Clusters in the calorimeters were interpreted as neutral particles if they were not associated to charged particles and if their energy exceeded 100 MeV. All charged and neutral particles that satisfy these criteria were considered good particles and they were used to compute the relevant event quantities. To assure good quality of the data, the ratio of good to total number of particles was required to be above 0.7. Particles that did not pass quality selection but had an associated calorimetric energy of at least 2 GeV had their angles taken from those of the track, but their momentum was recomputed from the energy of the calorimetric measurement (such particles were not included in the good sample). Events had to have between four and ten good charged particle tracks. In addition, it was required that the thrust be less than 0.99; the transverse momentum had to be bigger than 3 GeV/c, and $|\cos\theta_{p_{miss}}| < 0.95$ (polar angle of the missing momentum vector). Very forward-going events were eliminated by requiring E_{30} less than 70% of the total visible energy. With this preselection, the total number of simulated background events and real data events was reduced by a factor of about 6000. Only events passing these pre-selections were analysed further.

The selection takes advantage of the fact that signal events can be separated into two different kinematic regions of the $(m_{\tilde{\chi}_1^0}, m_{\tilde{l}})$ space: when the mass difference $\Delta m = m_{\tilde{\chi}_1^0} - m_{\tilde{l}}$ is bigger than about 10 GeV/c^2, all four leptons carry similar momenta. When the difference becomes smaller, the two leptons coming from the decay of the $\tilde{l}$ tend to be

the most energetic, increasingly so as the $\tilde{\chi}_1^0$ mass increases. The Durham algorithm [38] was used to divide the event into four jets by allowing the jet resolution parameter to vary as a free variable. Numbering the jets from 1 to 4 with $E_1 > E_2 > E_3 > E_4$, a variable r was defined as:

$$r = \frac{E_3 + E_4}{E_1 + E_2} \ . \tag{5}$$

The distribution of r shifts towards lower values with increasing neutralino masses.

At the preselection level the two main differences between the $\tilde{\tau}_1$ NLSP and $\tilde{l}_R$ co-NLSP scenarios come from the fact that the mean number of neutrinos carrying away undetected energy and momentum and the number of charged particles per event is considerably bigger for the former scenario.

In the $\tilde{\tau}_1$ NLSP scenario, the simulated background samples were then divided into two samples above and below $r = 0.1$ and different requirements were imposed in the two cases. No significant dependence on this variable was observed in the $\tilde{l}_R$ co-NLSP scenario. Two sets of cuts were applied in order to reduce the $\gamma\gamma$ and $f\bar{f}(\gamma)$ backgrounds and a third set of cuts to select events according to their topology. Those cuts are compiled in Table 6.

		$\tilde{\tau}_1$ NLSP		$\tilde{l}_R$ co-NLSP
		$r > 0.1$	$r \leq 0.1$	
Cuts against $\gamma\gamma$	E_T (GeV)	> 11	> 12	> 4
	E_{30} (GeV)	$< 0.6\sqrt{s}$	$< 0.6\sqrt{s}$	$< 0.6\sqrt{s}$
	m_{miss} (GeV)	$< 0.88\sqrt{s}$	$< 0.9\sqrt{s}$	$< 0.88\sqrt{s}$
	p_{max} (GeV/c)	> 4	> 3	> 8
	p_T (GeV/c)			> 6
Cuts against $f\bar{f}(\gamma)$	N_{good}	< 7	< 9	< 7
	T	< 0.975	< 0.975	< 0.95
	acoplanarity (°)	> 8	> 8	> 8
	m_{miss} (GeV)	$> 0.3\sqrt{s}$	$> 0.3\sqrt{s}$	$> 0.2\sqrt{s}$
Cuts based on topology	*jet-beam angle* (°)	> 17	> 17	> 18
	2-jets cone angle (°)	> 20	> 20	> 25
	4-jets separation (°)	> 8	> 4	> 9

Table 6: Sets of cuts applied in the search for neutralino pair production to eliminate the different background sources. p_{max} is the momentum of the charged particle with largest momentum; N_{good} is the number of good particles in the event; T is the event thrust; m_{miss} is the missing mass of the event. Signal events tend naturally to cluster into a 4-jet topology. Taking this into account, cuts based on topology were applied: *jet-beam angle* is the angle between the jet direction and the beam direction; *2-jets cone angle* represents the broadness of the 2-jets (considering only charged particles) obtained when reducing the 4-jet topology into a 2-jets configuration with the Durham algorithm; and finally, *4-jets separation* is the angle between jets.

After these cuts, an efficiency between 26 and 44% was obtained for the signal events in the $\tilde{\tau}_1$ NLSP scenario, and between 35 and 46% in the $\tilde{l}$ co-NLSP scenario. The number of events remaining in data and simulated samples after the selection procedure were 8 and 7.1±0.6 respectively in the $\tilde{\tau}_1$ NLSP scenario, and 7 and 6.6±0.6 respectively in the $\tilde{l}$ co-NLSP scenario.

4.3 Chargino pair production

The search for chargino pair production, $e^+e^- \rightarrow \tilde{\chi}_1^+\tilde{\chi}_1^- \rightarrow \tilde{l}^+\nu\tilde{l}^-\overline{\nu} \rightarrow l^+\nu\tilde{G}l^-\overline{\nu}\tilde{G}$, makes use, without modification, of four different analyses depending on the gravitino mass or, equivalently, on the mean decay length of the slepton. When the slepton decays at the vertex, the combination of two analyses can be exploited, the search for charginos and the search for acoplanar leptons in gravity mediated supersymmetry breaking scenarios. Details of these analyses can be found in [39,40]. For intermediate mean decay lengths of the slepton the topology is large impact parameter tracks or kinks, therefore, the two analyses explained in sections 4.1.1 and 4.1.2 can be used. Finally, if the slepton decays outside the tracking devices the signature corresponds to stable heavy leptons and this analysis is explained in section 4.4.

The selections developed for these searches were thus applied to simulated data samples with different gravitino masses, and the results are presented in terms of 95% confidence level (CL) excluded regions in the $(m_{\tilde{l}}, m_{\tilde{\chi}_1^+})$ plane in section 5.3.

4.4 Heavy stable charged particles search

In this analysis it is assumed that the slepton lifetime is large enough that the sleptons can pass through the tracking devices without decaying. If the sleptons are pair produced, one expects two slowly moving particles, which are characterized by an abnormally large energy loss in the TPC. Furthermore, no Cherenkov light is expected to be produced by them in the Ring Imaging CHerenkov detectors (RICH) of DELPHI. Both set of information are combined to identify such particles.

Only events with two or three charged particles were considered. Candidate particles were required to have hits both in the VD and in the TPC. The particle momentum had to be above 5 GeV/c^2, and the particle length was required to be at least 30 cm. To reduce cosmic rays background the absolute value of the particle impact parameter was required to be below 0.15 cm in the xy plane and 1.5 cm in z. Furthermore, the difference of the impact parameters in z of the two most energetic particles in the event was required to be less than 1 cm. An additional protection was added against showering electrons for which the particle extrapolation through the RICH can be unreliable. For charged particles with an associated electromagnetic energy exceeding 15 GeV, an additional hit in the Outer detector was required. A careful run selection ensured that the RICH detectors were fully operational.

The energy loss measurement was required to be based on at least 80 wires, and the dE/dx calibration was checked on a TPC sector by sector basis, using Z^0 calibration data of the same year.

Events were selected if they contained at least one charged particle with:
(I) momentum above 5 GeV/c, high ionization loss in the TPC and no associated γs in the gas radiator of the RICH (gas veto) or,
(II) momentum above 15 GeV/c, ionization loss at least 0.3 below the expectation for a proton and surviving the gas veto or,
(III) momentum above 15 GeV/c, surviving the gas and the liquid RICH veto.
An event was also selected if the two particles with the highest momentum were characterized by a high ionization loss or a gas veto, or if both particles had a low ionization loss. Special care has been taken about the dE/dx in sector 6 (S6) of the Time Projection Chamber which was not operational during the second half of data taking in 2000, reducing the efficiency of the search by several percent as the dE/dx search windows could not be applied to particles pointing to S6. To recover some sensitivity for particles

pointing to this sector, only the double veto search window was applied, requiring hits in the Vertex Detector, Inner Detector and Outer Detector to ensure a good propagation of the particles through the RICH.

The data of the year 2000 has been subdivided into 3 energy bins, corresponding to energies below 206 GeV (85 pb^{-1}), between 206 GeV and 207 GeV (124 pb^{-1}), and above 207 GeV (11.4 pb^{-1}). A total background of 0.25±0.04 events was estimated from data itself by counting the number of particles passing the individual selection criteria.

No candidate events were selected in data. Figure 7 shows the data and the three main search windows. The expectation for a 95 GeV/c^2 mass signal is also shown. Signal efficiencies were estimated from simulation. For particle masses between 10 GeV/c^2 and 60 GeV/c^2 the signal efficiencies are of the order of 30%. For larger masses they rise with increasing mass to about 76-78%. Then the efficiency drops rapidly when approaching the kinematic limit, and it is assumed to be zero at the kinematic limit.

4.5 Sgoldstino search

This section describes the search for $e^+e^- \rightarrow \phi\gamma$ events, with the sgoldstino going to two gammas or two gluons. The two channels considered here give rise to two different topologies. On the one hand, if the sgoldstino decays into two photons, the final topology of the event is three high energy photons, one of them monochromatic. On the other hand, if the sgoldstino decays into two gluons, one monochromatic photon and two jets can be expected in the final state.

4.5.1 $\phi \rightarrow \gamma\gamma$ channel

Events were selected as $\gamma\gamma\gamma$ candidates if they had at least two electromagnetic energy clusters with $0.219 < E/\sqrt{s} < 0.713$; at least another one with $E > 5$ GeV and no more than two additional clusters, the second (if present) with $E < 5$ GeV. The two most energetic electromagnetic clusters had to be in the HPC region, $42^\circ < \theta < 89^\circ$ ($91^\circ < \theta < 138^\circ$), or in the FEMC region, $25^\circ < \theta < 32.4^\circ$ ($147.6^\circ < \theta < 155^\circ$). Finally, the third cluster had to be in the region $\theta > 42^\circ$ ($\theta < 138^\circ$) or $20^\circ < \theta < 35^\circ$ ($145^\circ < \theta < 160^\circ$). The event should not have hits in two of the three Vertex Detector layers compatible (within $\pm 2^\circ$ in the azimuthal direction) with the extrapolated trajectory of a particle from the beam crossing point to an electromagnetic cluster in the calorimeters.

Further, two hemispheres were defined by a plane orthogonal to the direction of the most energetic cluster. One hemisphere was required to have no charged particles detected in the barrel region of the tracking devices other than the VD with a momentum greater than 1 GeV/c extrapolating to within 5 cm of the mean beam crossing point. The requirement was further strengthened to suppress the larger e^+e^- background, by demanding that both hemispheres had no such particle detected by the TPC with $\theta < 35^\circ$.

The events obtained after this selection had a three-body final state kinematics if there was no significant initial state radiation lost along the beam pipe. Defining $\Delta = |\delta_{12}| + |\delta_{13}| + |\delta_{23}|$, where δ_{ij} is the angle between the particles i and j, Δ should be 360° in a three-body final state since the particles lie in a plane. If only the events with $\Delta > 358^\circ$ were accepted, the energies of the particles could then be determined with very good precision on the basis of the measured photon directions:

$$E_1 = \sqrt{s}\frac{\sin\delta_{23}}{\delta};\ E_2 = \sqrt{s}\frac{\sin\delta_{13}}{\delta};\ E_3 = \sqrt{s}\frac{\sin\delta_{12}}{\delta} \qquad (6)$$

with $\delta = \sin\delta_{12}+\sin\delta_{13}+\sin\delta_{23}$. The error on the energy evaluation was further minimised by requiring $\min(\delta_{12},\delta_{13},\delta_{23}) > 2^\circ$.

In $\phi\gamma$ events the ϕ decay products are expected to be isotropically distributed in the ϕ centre-of-mass system. This fact implies that the distribution of $cos\alpha$, where α is the angle between the ϕ direction (opposite to the prompt photon) and the direction of one of the two ϕ decay products, in the ϕ centre-of-mass system, should be flat. On the other hand, in the QED background, $|cos\alpha|$ peaks at 1 and therefore only the combinations giving $|cos\alpha| < 0.9$ were accepted.

The number of selected events giving up to three combinations and the expected background were 22 and $20.3^{+1.5}_{-1.9}$, respectively. The error on the background was due to a correction applied in order to take into account the missing higher orders (additional radiation above α^3 which gives events having low values of Δ) in the simulation of the QED background. These kind of events were removed only from the selected sample of real data and therefore, a corresponding normalization correction factor of $(-13^{+4}_{-7})\%$ was applied to the simulated sample. This correction is the dominant contribution to the systematic error. No significant background in addition to $e^+e^- \to \gamma\gamma(\gamma)$ events was found.

No significant variation in the acceptance for a $\phi\gamma$ signal and in the selection efficiency inside the acceptance region were observed in the 2000 data with respect to the lower energies in previous years: acceptance $(51 \pm 2)\%$ and efficiency $(76.6 \pm 2.5)\%$.

The energy resolution remained also unchanged and it was better than 0.5% over the whole photon energy range.

The photon recoil mass spectrum obtained for the events collected during the 2000 run including those reported in [2] is shown in Figure 8-a. The data are superimposed on the expected QED background distribution.

4.5.2 $\phi \to gg$ channel

This channel is expected to give a final state with one photon and two jets. An event was selected as a γgg candidate if it had an electromagnetic energy cluster identified as photon with $E > 5$ GeV and $\theta > 20^\circ$. The event must not have electromagnetic clusters below $\theta = 5^\circ$. The total multiplicity (charged and neutral) had to be greater than 10, and the charged multiplicity greater than 5. To remove $\gamma\gamma$ events the cut $\sum_{i=1}^{n}\sqrt{(p_x^2+p_y^2)_i} > 0.125\sqrt{s}$ (where n is the total multiplicity) was used. The sum of the absolute values of all particle momenta along the thrust axis had to be greater than $0.20\sqrt{s}$. An electromagnetic cluster with $E < 0.45\sqrt{s}$, or a total particle multiplicity greater than 16 when the cluster energy was greater than $0.45\sqrt{s}$ had to be present. The polar angle of the missing momentum had to satisfy $|cos(\theta_{p_{miss}})| < 0.995$. The visible energy had to be greater than $0.60\sqrt{s}$. The jets had to be incompatible with the $b\bar{b}$ hypothesis by requiring the combined btag of the events to be less than zero [41]. Finally, the aforementioned $|\cos\alpha|$ and Δ had to be less than 0.9 and greater than 350°, respectively.

The events were reconstructed forcing all particles but the photon into a 2-jet topology using the Durham [38] algorithm. Events were removed if $y_{cut} > 0.02$. The events were also rejected if the angle between the photon and the nearest jet was less than 10°. In the case of more than one photon candidate in the event, the most energetic one was considered as the one produced in $e^+e^- \to \phi\gamma$.

Similar to the $\gamma\gamma\gamma$ selection, the events obtained after this selection were three-body final state events in absence of additional lost radiation. Therefore kinematic constraints

were applied here as well. In this case, however, the jet direction was determined with a poorer precision than that obtained for photons, therefore the cut in Δ was less stringent and the resolution for the reconstructed photon energy was poorer: a two-Gaussian fit gave $\sigma_1 = 1.2$ GeV (55% of the area) and $\sigma_2 = 4.1$ GeV.

The number of selected events and the expected background were 766 and 775 ± 5, respectively.

No significant variation in the acceptance and in the selection efficiency inside the acceptance region was observed in the 2000 data compared to the values at lower energies. The acceptance was $(76 \pm 2)\%$ (almost independent of m_ϕ) and the efficiency ranged from 20 to 55% depending on the photon energy. The energy resolution was also unchanged.

The photon recoil mass spectrum obtained for the events collected during the 2000 run and including those reported in [2] is shown in Figure 8-b. The data are superimposed on the expected background distribution.

5 Results and interpretation

Since there was no evidence for a signal above the expected background, the number of candidates in data and the expected number of background events were used to set limits at the 95% confidence level (CL) on the pair production cross-section and masses of the sparticles searched for. The model described in reference [42] was used to derive limits within the GMSB scenarios. This model assumes radiatively broken electroweak symmetry and null trilinear couplings at the messenger scale. The corresponding parameter space was scanned as follows: $1 \leq n \leq 4$, 5 TeV $\leq \Lambda \leq$ 90 TeV, $1.1 \leq M/\Lambda \leq 10^9$, $1.1 \leq \tan\beta \leq 50$, and $sign(\mu) = \pm 1$. The meaning of the parameters is explained in section 1. The limits presented here are at $\sqrt{s} = 208$ GeV after combining these results with those of the searches at lower centre-of-mass energies using the likelihood ratio method [43].

5.1 Slepton pair production

The results of the search for slepton pair production are presented in the ($m_{\tilde{G}}$,$m_{\tilde{l}}$) plane in Figure 9-a combining the impact parameter, the kink and the stable heavy lepton analyses, and using all DELPHI data from 130 GeV to 208 GeV centre-of-mass energies [1,32–34].

The $\tilde{\tau}_1$ pair production cross-section depends on the mixing in the stau sector. Therefore, in order to put limits on the $\tilde{\tau}_1$ mass, the mixing angle had to be fixed. The results presented here correspond to a mixing angle in the stau sector which gives the minimum $\tilde{\tau}_1$ pair production cross-section. Within the $\tilde{\tau}_1$ NLSP scenario, the impact parameter and kink analyses extended the limit $m_{\tilde{\tau}_1} > 82.5$ GeV/c^2 for $m_{\tilde{G}} \lesssim 6$ eV/c^2, set by MSUGRA searches [12], up to $m_{\tilde{G}} = 600$ eV/c^2, reaching the maximum excluded value of $m_{\tilde{\tau}_1} = 93.6$ GeV/c^2 for $m_{\tilde{G}} = 130$ eV/c^2. For $m_{\tilde{G}} > 130$ eV/c^2 the best lower mass limit was set by the stable heavy lepton search. Although not shown in the figures, DELPHI excludes $m_{\tilde{G}}$ from $3{\cdot}10^{-4}$ eV/c^2 to 0.2 eV/c^2. $m_{\tilde{\tau}_1}$ masses below 40 GeV/c^2 have been already excluded as discussed in [32].

Within the sleptons co-NLSP scenario, the cross-section limits were used to derive lower limits for $\tilde{l}_R$ (Figure 9-b) masses at 95% CL. Assuming mass degeneracy between the sleptons, the kink and impact parameter searches extended the limit $m_{\tilde{l}_R} > 88$ GeV/c^2 set by MSUGRA searches [12] for very short NLSP lifetimes up to $m_{\tilde{G}} = 800$ eV/c^2. For the MSUGRA case the best limit from the $\tilde{\mu}_R$ has been used. The maximum excluded value

of $m_{\tilde{l}_R}$= 96.5 GeV/c^2 was achieved for $m_{\tilde{G}}$= 150 eV/c^2. For $m_{\tilde{G}} > 150$ eV/c^2 the best lower mass limit was set by the stable heavy lepton search. $\tilde{l}_R$ masses below 40 GeV/c^2 were excluded by LEP1 data [44]. In the case of $\tilde{l}_R$ degeneracy, this limit improved to 43 GeV/c^2.

5.2 Neutralino pair production

Limits for neutralino pair production cross-section were derived in the $\tilde{\tau}_1$ NLSP and sleptons co-NLSP scenarios for each ($m_{\tilde{\chi}^0_1}$,$m_{\tilde{l}}$) combination for $m_{\tilde{G}}$ below a few eV/c^2. For the $\tilde{\tau}_1$ NLSP case the combination took into account the results from the LEP runs from 1996 (for $\sqrt{s} \geq 161$ GeV) to 2000 [1,32,33]. The limits for the production cross-section allowed some sectors of the ($m_{\tilde{\chi}^0_1}$, $m_{\tilde{l}}$) space to be excluded. In order to exclude as much as possible of the mass plane, the results from two other analyses were taken into account. The first is the search for slepton pair production in the context of MSUGRA models. From the experimental lower limit on the mass of the $\tilde{\tau}_1$ set by that search, $m_{\tilde{\tau}_1} > 82.5$ GeV/c^2 [12], it can be concluded that at least neutralino masses below the lower bound for $m_{\tilde{\tau}_1}$ plus the tau mass are excluded. The second is the search for lightest neutralino pair production in the region of the mass space where $\tilde{\chi}^0_1$ is the NLSP [13] (the region above the diagonal line in Figure 10, i.e. $m_{\tilde{\tau}_1} > m_{\tilde{\chi}^0_1}$). Within this zone, the neutralino decays into a gravitino and a photon.

As an illustration, Figure 10 presents the 95% CL excluded areas for $m_{\tilde{G}} < 1$ eV/c^2 in the $m_{\tilde{\chi}^0_1}$ vs $m_{\tilde{\tau}_1}$ plane for the $\tilde{\tau}_1$ NLSP scenario and for different values of the number of messenger generations (n). The positive-slope dashed area is excluded by the neutralino pair production search. The negative-slope dashed area is excluded by the analysis searching for neutralino pair production followed by the decay $\tilde{\chi}^0_1 \rightarrow \tilde{G}\gamma$. The point-hatched area is excluded by the direct search for slepton pair production within MSUGRA scenarios. The neutralino mass range is plotted up to almost the kinematic limit.

5.3 Chargino pair production

Limits on the production cross-section for chargino pairs were derived for each ($m_{\tilde{G}}, m_{\tilde{l}}, m_{\tilde{\chi}^+_1}$) combination for $m_{\tilde{G}}$ below a few eV/c^2. Figure 11 (a) shows, as an example, the 95% CL upper limit on the chargino pair production cross-section at $\sqrt{s}$ = 208 GeV as a function of $m_{\tilde{\chi}^+_1}$ and $m_{\tilde{l}_R}$ after combining with the results of the searches for large impact parameter and kink at lower energies using the likelihood ratio method [43], for $m_{\tilde{G}}$ = 100 eV/c^2. The limits on the chargino pair production cross-section were used to exclude areas within the ($m_{\tilde{\chi}^+_1}$, $m_{\tilde{l}}$) plane for different domains of the gravitino mass, combining results from all the centre-of-mass energies from 183 GeV to 208 GeV [1,32,35]. Figure 11 also shows the regions excluded at 95% CL in the ($m_{\tilde{\chi}^+_1}$,$m_{\tilde{\tau}_1}$) plane, for the $\tilde{\tau}_1$ NLSP scenario (b), and in the ($m_{\tilde{\chi}^+_1}$,$m_{\tilde{l}_R}$) plane, for the $\tilde{l}_R$ co-NLSP scenario (c). The positive-slope area is excluded for $m_{\tilde{G}} > 1$ eV/c^2. This limit is also valid for smaller masses of the gravitino because they lead to the same final state topologies. The negative-slope area is only excluded for $m_{\tilde{G}} > 100$ eV/c^2. The areas below $m_{\tilde{\tau}_1}$= 82.5 GeV/c^2 in the $\tilde{\tau}_1$ NLSP scenario, and below $m_{\tilde{l}_R}$= 88 GeV/c^2 in the $\tilde{l}_R$ co-NLSP scenario, are excluded by the direct search for slepton pair production

in MSUGRA models [12]. These lower bounds on $m_{\tilde{\tau}_1}$ and $m_{\tilde{l}_R}$ from MSUGRA mean a limit on the $m_{\tilde{\chi}_1^\pm}$ at 82.5 GeV/c^2 and 88 GeV/c^2, respectively. In Figure 11 the exclusion regions given by the search for charginos in GMSB scenarios start at those values. The area of $\Delta m \leq 0.3$ GeV/c^2 is not excluded because in this region the charginos do not decay mainly to $\tilde{\tau}_1$ and ν_τ, but to W and $\tilde{G}$. Thus, if $\Delta m \geq 0.3$ GeV/c^2, the chargino mass limits are 100 GeV/c^2 for all $m_{\tilde{G}}$, and 102 GeV/c^2 for $m_{\tilde{G}} > 100$ eV/c^2, in the $\tilde{\tau}_1$ NLSP scenario. In the sleptons co-NLSP scenario the limits are 96 GeV/c^2 for $m_{\tilde{G}} = 1$ eV/c^2, and 102 GeV/c^2 for $m_{\tilde{G}} > 100$ eV/c^2. The chargino mass limit decreases with decreasing $m_{\tilde{\tau}_1}$ because in scenarios with gravitino LSP small stau masses correspond to small sneutrino masses (both are proportional to Λ) and hence to smaller production cross-sections due to the destructive interference between the s- and t-channels.

It should be noticed that within the parameter space studied here, the lightest chargino is at least 40% heavier than the lightest neutralino. Thus, for small gravitino masses the search for neutralinos implies a lower limit on the lightest chargino of 130 GeV/c^2. Neutralinos are not directly searched for in heavier gravitino mass regions and therefore for this range of gravitino masses the limit of 102 GeV/c^2 for the chargino mass remains valid.

5.4 Heavy stable charged particle pair production

The results presented in section 4.4 were combined with previous DELPHI results in this channel [1,36,37], and cross-section limits were derived within MSSM models as indicated in Figure 12. From the intersection points with the predicted cross-sections for smuon or staus in the MSSM, left(right) handed smuons and staus can be excluded up to masses of 97.7(97.4) GeV/c^2 at 95%CL. No limits are given on selectrons here because the cross-section can be highly suppressed by an additional t-channel sneutrino exchange contribution.

5.5 Sgoldstino production

No excess of events nor clear evidence of an anomalous production of events with monochromatic photons is observed in either of the two channels. Therefore a limit on the cross-section of the new physics reaction contributing to the two topologies was set.

The number of detected events, the background rate and the detection efficiency depend on the ϕ mass. In addition, when the expected total width for the same m_ϕ value is comparable or larger than the experimental resolution, the data were compared with the background events in a region corresponding to 80% of the signal area. As a consequence, the limit on the signal cross-section depends on m_ϕ and $\sqrt{F}$. Furthermore, to take into account the different sensitivities of the two analysed channels, the likelihood ratio method was used [43]. Since the expected ϕ branching ratio and total width depend on the mass parameters as explained above, the 95% CL cross-section limit was computed as a function of m_ϕ and $\sqrt{F}$ for the two sets of parameters listed in Table 1, and is shown in Figure 13. By comparing the experimental limits with the expected production cross-section, it is possible to determine a 95% CL excluded region on the parameter space as shown in Figure 14. As explained in [18], to keep the particle interpretation the total width Γ must be much smaller than m_ϕ and therefore the region with $\Gamma > 0.5 m_\phi$ was not considered. In Figures 13 and 14 the sgoldstino mass range starts at 10 GeV/c^2 to avoid all theoretical subtleties connected with the non-perturbative aspects of the strong interaction. The upper value of the mass range approaches the kinematic Al limit.

5.6 Limits on the GMSB parameter space

Finally, all these results can be combined to produce exclusion plots within the $(\tan\beta, \Lambda)$ space. The corresponding parameter space was scanned as follows: $1 \leq n \leq 4$, 5 TeV $\leq \Lambda \leq$ 90 TeV, $1.1 \leq M/\Lambda \leq 10^9$, $1.1 \leq \tan\beta \leq 50$, and $sign(\mu) = \pm 1$. As an example, Figure 15 shows the zones excluded for n =1 to 4 for $m_{\tilde{G}} \leq 1$ eV/c^2, which corresponds to the NLSP decaying at the main vertex. The shaded areas are excluded. The areas below the dashed lines contain points of the GMSB parameter space with $\tilde{\chi}_1^0$ NLSP. The areas to the right (above for $n = 1$) of the dashed-dotted lines contain points of the GMSB parameter space where sleptons are the NLSP. It can be seen that the region of slepton NLSP increases with n. The contrary occurs to the region of neutralino NLSP.

The shaded areas below the dashed lines are excluded by the search for neutralino pair production followed by the decay $\tilde{\chi}_1^0 \rightarrow \tilde{G}\gamma$ (acoplanar photons search). However, the solid and almost vertical line that sets the lowest limit to the parameter Λ, is defined by the combination of the search for acoplanar photons, right handed selectrons with sleptons NLSP and neutralino pair production with stau NLSP. Finally, the search for stau NLSP improves the exclusion limit represented by the solid line with positive slope.

Theoretical arguments constrain the value of $\tan\beta$ to be between ~ 1.2 and ~ 65 [8]. A lower limit is set for the variable Λ at 17.5 TeV.

6 Summary

Lightest neutralino, slepton and chargino pair production were searched for in the context of light gravitino models. Two possibilities were explored: the $\tilde{\tau}_1$ NLSP and the sleptons co-NLSP scenarios. No evidence for signal production was found. Hence, the DELPHI collaboration sets lower limits at 95% CL for the mass of the $\tilde{\chi}_1^0$ as a function of the slepton masses, and lower mass limits for the sleptons in all the gravitino mass range. The limit on the chargino mass is 100 GeV/c^2 for all $m_{\tilde{G}}$ in the $\tilde{\tau}_1$ NLSP scenario and 96 GeV/c^2 in the sleptons co-NLSP scenario. All these results were combined to set limits on the GMSB parameter space. Combining all the data up to 208 GeV, a lower limit is set for the variable Λ at 17.5 TeV. Similar results have been obtained by the ALEPH experiment concerning all these searches [45].

Mass limits for heavy stable charged particles were also derived within the MSSM. For these particles the DELPHI collaboration sets lower mass limits at 95% CL for the left (right) handed stau and smuon at 97.7 (97.4) GeV/c^2.

Finally, cross-section and mass limits were derived for sgoldstinos at 95% CL since no evidence of an anomalous production of events with monochromatic photons was observed in either of the two channels.

Acknowledgements

We are greatly indebted to our technical collaborators, to the members of the CERN-SL Division for the excellent performance of the LEP collider, and to the funding agencies for their support in building and operating the DELPHI detector.
We acknowledge in particular the support of
Austrian Federal Ministry of Education, Science and Culture, GZ 616.364/2-III/2a/98,
FNRS–FWO, Flanders Institute to encourage scientific and technological research in the

industry (IWT), Belgium,
FINEP, CNPq, CAPES, FUJB and FAPERJ, Brazil,
Czech Ministry of Industry and Trade, GA CR 202/99/1362,
Commission of the European Communities (DG XII),
Direction des Sciences de la Matière, CEA, France,
Bundesministerium für Bildung, Wissenschaft, Forschung und Technologie, Germany,
General Secretariat for Research and Technology, Greece,
National Science Foundation (NWO) and Foundation for Research on Matter (FOM), The Netherlands,
Norwegian Research Council,
State Committee for Scientific Research, Poland, SPUB-M/CERN/PO3/DZ296/2000, SPUB-M/CERN/PO3/DZ297/2000, 2P03B 104 19 and 2P03B 69 23(2002-2004)
JNICT–Junta Nacional de Investigação Científica e Tecnológica, Portugal,
Vedecka grantova agentura MS SR, Slovakia, Nr. 95/5195/134,
Ministry of Science and Technology of the Republic of Slovenia,
CICYT, Spain, AEN99-0950 and AEN99-0761,
The Swedish Natural Science Research Council,
Particle Physics and Astronomy Research Council, UK,
Department of Energy, USA, DE-FG02-01ER41155.

References

[1] DELPHI Collaboration, P. Abreu *et al.*, Phys. Lett. **B503** (2001) 34.
[2] DELPHI Collaboration, P. Abreu *et al.*, Phys. Lett. **B494** (2000) 203.
[3] S. Dimopoulos, S. Thomas, J.D. Wells, Nucl. Phys. **B488** (1997) 39.
[4] S. Ambrosanio, G.D. Kribs, S.P. Martin, Phys. Rev. **D56** (1997) 1761.
[5] G.F. Giudice, R. Rattazzi, Phys. Rep. **322** (1999) 419 and Phys. Rep. **322** (1999) 501.
[6] D.A. Dicus and S. Nandi, Phys. Rev. **D56** (1997) 4166.
[7] H. Pagels and J.R. Primack, Phys. Rev. Lett. **48** (1982) 223;
S. Weinberg, Phys. Rev. Lett. **48** (1982) 1303;
T. Asaka, K. Hamaguchi and K. Suzuki, Phys. Lett. **B490** (2000) 136.
[8] S. P. Martin, hep-ph/9709356, Perspectives on Supersymmetry, ed. by G. Kane, Worldscientific, Singapore (1998) pp 1-98.
[9] S. Dimopoulos, M. Dine, S. Raby, S. Thomas and J. D. Wells, Nucl. Phys. Proc. Suppl. **A52** (1997) 38.
[10] E. Calzetta, A. Kandus, F. D. Mazzitelli and C. E. M. Wagner, Phys. Lett. **B472** (2000) 287.
[11] A. Bartl *et. al.*, Z. Phys. **C73** (1997) 469.
[12] EP Paper 302/Draft 2 (9 July 2002) (To be submitted to Eur. Phys. J. C).
[13] DELPHI Collaboration, P. Abreu *et al.*, Eur. Phys. J. **C17** (2000) 53;
DELPHI Collaboration, P. Abreu *et al.*, Eur. Phys. J. **C6** (1999) 371.
[14] B. Abbott *et al.*, Phys. Rev. Lett. **80** (1998) 442.
[15] K. Cheung, D. A. Dicus, B. Dutta, S. Nandi, Phys. Rev. **D58** (1998) 15008.
[16] H. Dreiner, hep-ph/9707435, Perspectives on Supersymmetry, ed. by G. Kane, Worldscientific, Singapore (1998) pp 462-479.
[17] DELPHI Collaboration, P. Abreu *et al.*, Phys. Let. **B485** (2000) 95.
[18] E. Perazzi, G. Ridolfi and F. Zwirner, Nucl. Phys. **B574** (2000) 3.
[19] DELPHI Collaboration, P. Aarnio *et al.*, Nucl. Instr. and Meth. **303** (1991) 233.
[20] DELPHI Collaboration, P. Abreu *et al.*, Nucl. Instr. and Meth. **378** (1996) 57.
[21] The DELPHI Trigger Group, A. Augustinus *et al.*, *The DELPHI Trigger System at LEP2* (to be submitted to Nucl.Instr.and.Meth. A).
[22] T. Sjöstrand, Comp. Phys. Comm. **39** (1986) 347;
T. Sjöstrand, `PYTHIA 5.6` *and* `JETSET 7.3`, CERN-TH/6488-92.
[23] DELPHI Collaboration, P. Abreu *et al.*, Z. Phys. **C73** (1996) 11.
[24] SUSYGEN 2.20, S. Katsanevas and S. Melachroinos in *Physics at LEP2*, CERN 96-01, **Vol. 2**, p. 328 and http://lyoinfo.in2p3.fr/susygen/susygen.html;
S. Katsanevas and P. Moravitz, Comp. Phys. Comm. **122** (1998) 227.
[25] F.A. Berends and R. Kleis, Nucl. Phys. **B186** (1981) 22.
[26] S. Jadach, B.F.L. Ward and Z. Was, Comp. Phys. Comm. **79** (1994) 503.
[27] S. Jadach, W. Placzek, B.F.L. Ward, Phys. Lett. **B390** (1997) 298.
[28] F.A. Berends, R. Pittau, R. Kleiss, Comp. Phys. Comm. **85** (1995) 437.
[29] J. Fujimoto *et al.*, Comp. Phys. Comm. **100** (1997) 128.
[30] T. Alderweireld *et al.*, in *LEP2 MCWorkshop*, CERN-2000-009, p 219.
[31] F.A. Berends, P.H. Daverveldt, R. Kleiss, Comp. Phys. Comm. **40** (1986) 271, Comp. Phys. Comm. **40** (1986) 285, Comp. Phys. Comm. **40** (1986) 309.
[32] DELPHI Collaboration, P. Abreu *et al.*, Eur. Phys. J. **C16** (2000) 211.
[33] DELPHI Collaboration, P. Abreu *et al.*, Eur. Phys. J. **C7** (1999) 595.
[34] DELPHI Collaboration, P. Abreu *et al.*, Eur. Phys. J. **C6** (1999) 385.

[35] DELPHI Collaboration, P. Abreu *et al.*, Phys. Lett. **B466** (1999) 61.
[36] DELPHI Collaboration, P. Abreu *et al.*, Phys. Lett. **B478** (2000) 65.
[37] DELPHI Collaboration, P. Abreu *et al.*, Phys. Lett. **B444** (1998) 491.
[38] S. Catani, Phys. Lett. **B269** (1991) 432.
[39] DELPHI Collaboration, P. Abreu *et al.*, Phys. Lett. **B479** (2000) 129.
[40] DELPHI Collaboration, P. Abreu *et al.*, Eur. Phys. J. **C19** (2001) 29.
[41] DELPHI Collaboration, P. Abreu *et al.*, Phys. Lett. **B462** (1999) 425.
[42] D. A. Dicus, B. Dutta, S. Nandi, Phys. Rev. **D56** (1997) 5748;
D. A. Dicus, B. Dutta, S. Nandi, Phys. Rev. Lett. **78** (1997) 3055.
[43] A.L. Read, *Modified Frequentist Analysis of Search Results (The CLs Method)*, CERN-OPEN-2000-205, 81.
[44] Particle Data Group, D.E. Groom *et al.*, Eur. Phys. J. **C15** (2000) 1.
[45] ALEPH Collaboration, A. Heister *et al.*, CERN EP 2002-021, hep-ex 0203024, (subm. to Eur. Phys. J.).

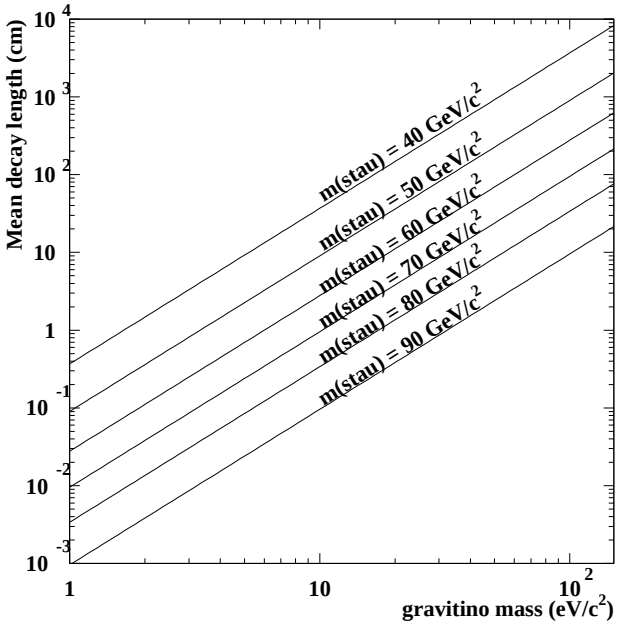

Figure 1: $\tilde{\tau}$ mean decay length ($\hat{L} = c\tau\gamma\beta$) as a function of the gravitino mass for different $\tilde{\tau}$ mass values.

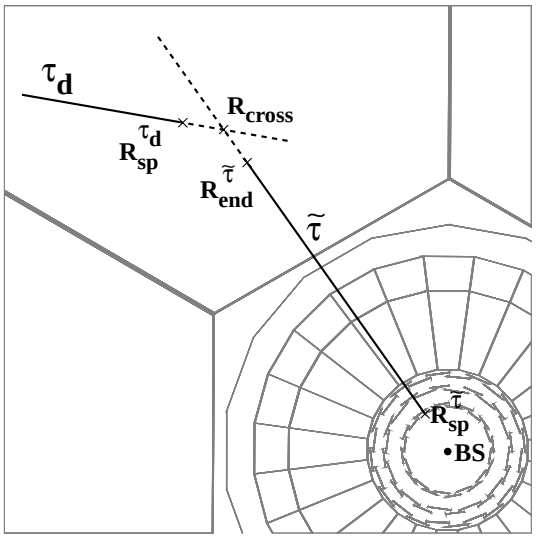

Figure 2: Sketch illustrating the reconstruction of a secondary vertex in the plane perpendicular to the beam direction. All the radii are measured with respect to the beam spot (BS).

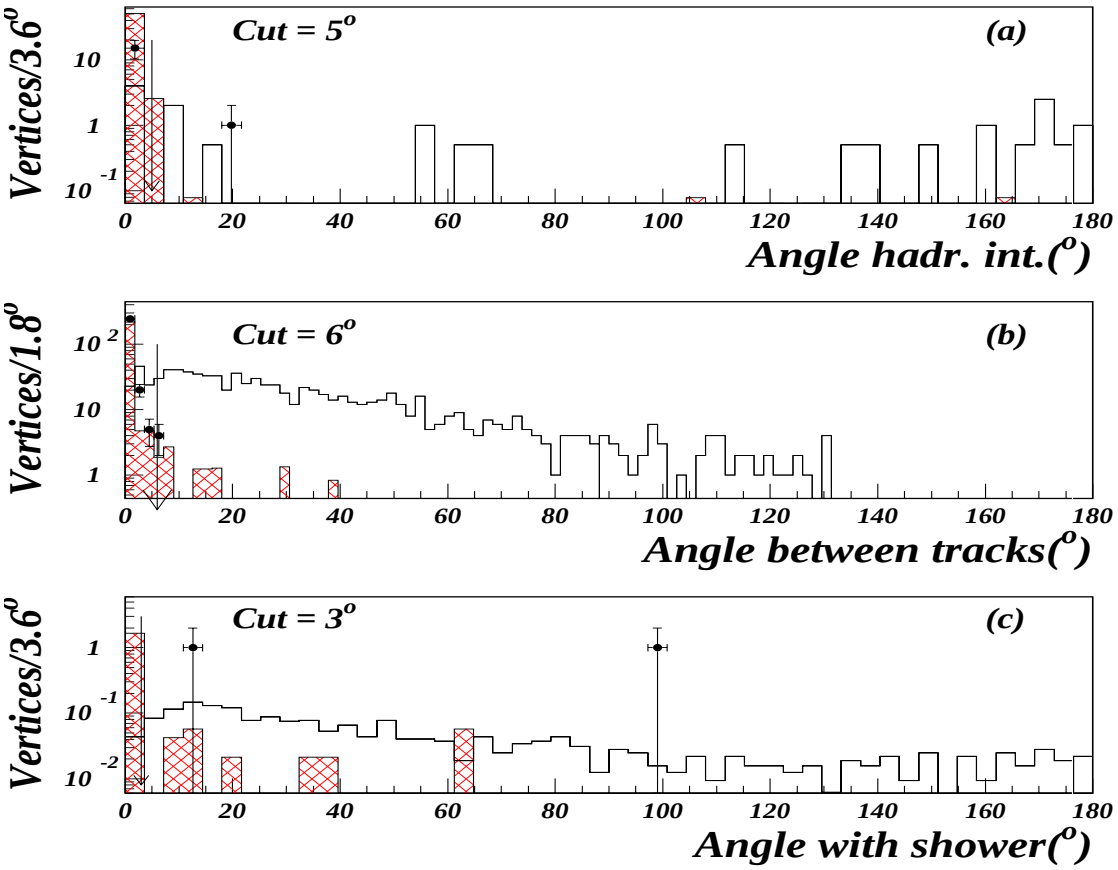

Figure 3: (a) Angle between the directions defined by the hadronic vertex and the reconstructed vertex w.r.t. beam spot, (b) angle between the tracks of the kink, and (c) angle between the electromagnetic shower and the missing momentum. Dots are real data, cross-hatched histogram is the SM background and blank histogram is the simulated signal ($m_{\tilde{\tau}_1} = 60$ GeV/c^2, $\hat{L} = 50$ cm and $\sqrt{s} = 208$ GeV).

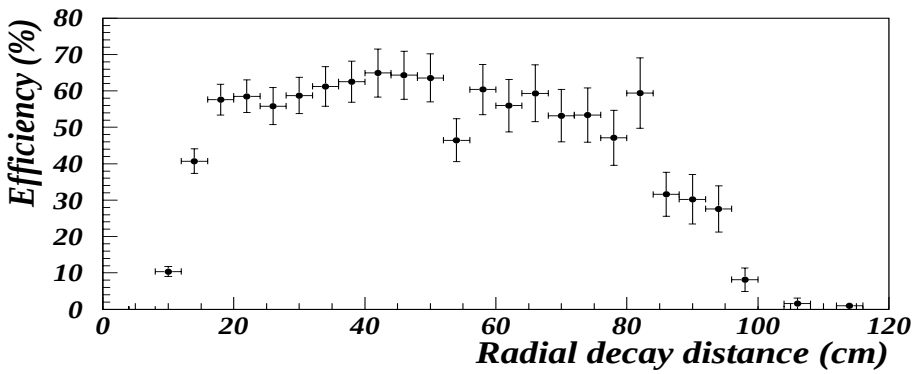

Figure 4: Efficiency as a function of the decay radius for a sample of staus with $\hat{L} = 50$ cm and $\sqrt{s} = 208$ GeV.

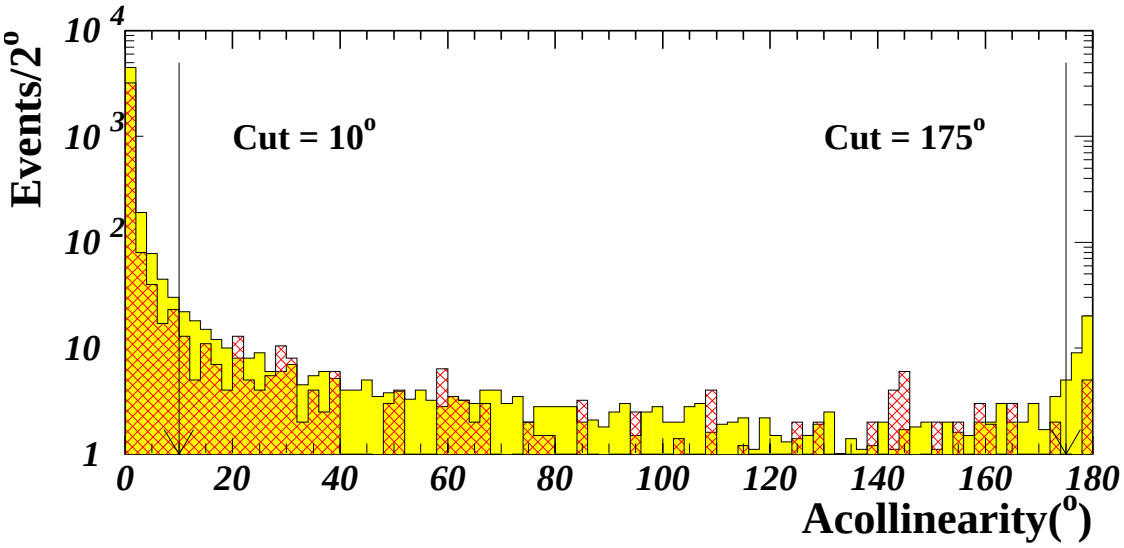

Figure 5: Acollinearity distribution for real data minus expected SM background (cross-hatched histogram), compared to cosmic ray events shown in dark grey. The cuts on this variable are shown with arrows.

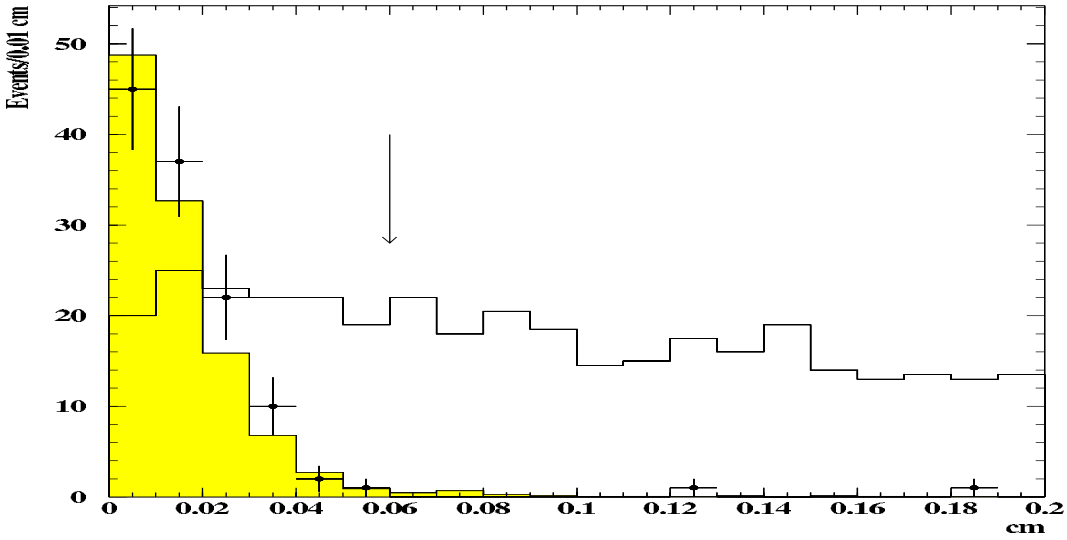

Figure 6: $\sqrt{b_1^2 + b_2^2}$ distribution for data (dots), simulated SM backgrounds (grey histogram) and simulated signal of $m_{\tilde{\tau}_1} = 90$ GeV/c^2 and $m_{\tilde{G}} = 25$ eV/c^2 at $\sqrt{s} = 206$ GeV and a boosted mean decay length ~ 1 cm (white histogram, in arbitrary scale) after all other cuts applied by the small impact parameter search.

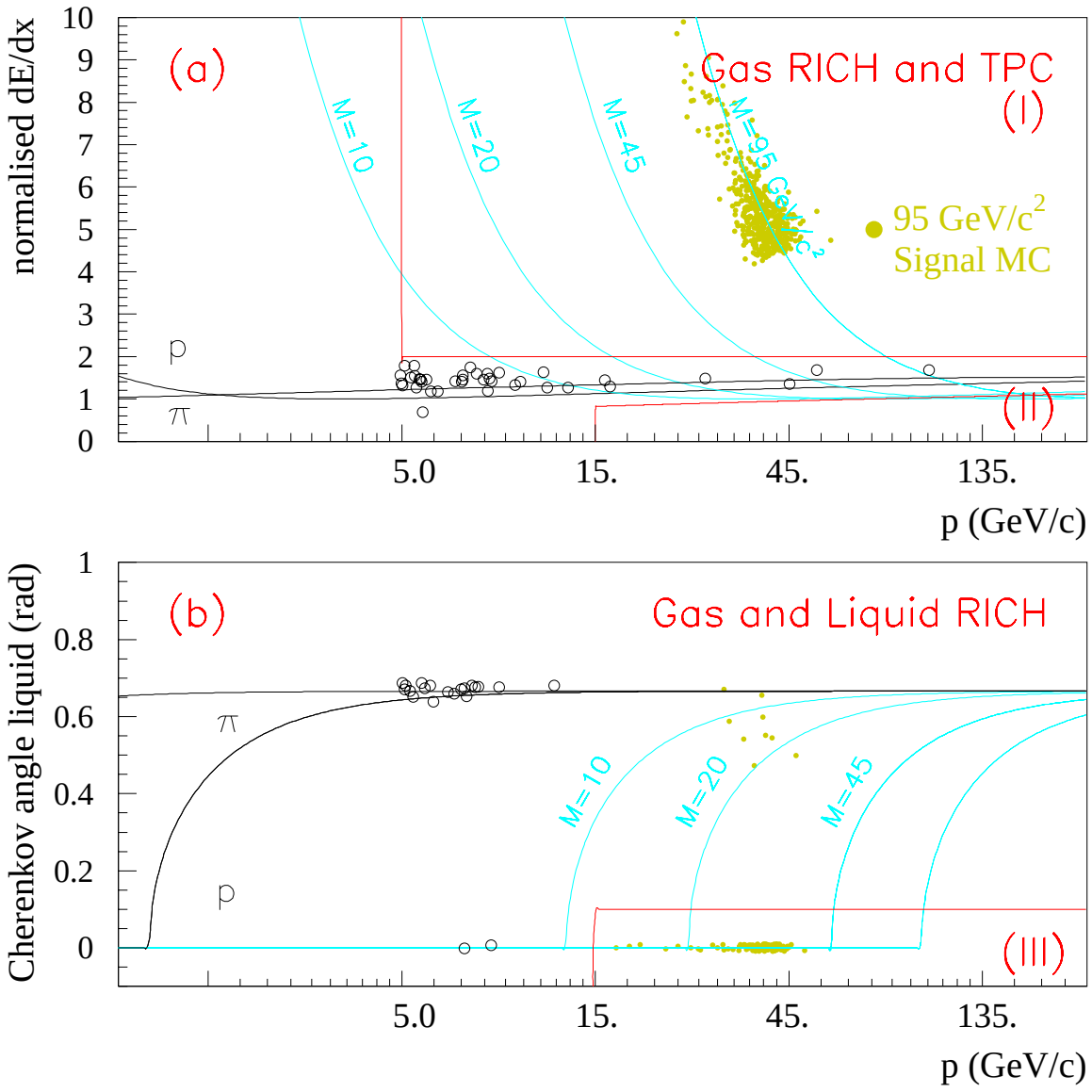

Figure 7: (a) Normalised energy loss as a function of the momentum after the gas veto for the 208 GeV data. (b) Measured Cherenkov angle in the liquid radiator as a function of the momentum after the gas veto: if four photons or less were observed in the liquid radiator, the Cherenkov angle was set equal to zero. The areas labelled (I), (II) and (III) indicate the selection criteria explained in the text. Open circles are data. The small filled circles indicate the expectation for a 95 GeV/c^2 mass signal with charge $\pm$e, resulting in a large dE/dx (upper plot) and no photons (except for a few accidental rings) in the liquid Cherenkov counter (lower plot). The solid lines with a mass signal value indicate the expectation for heavy stable sleptons.

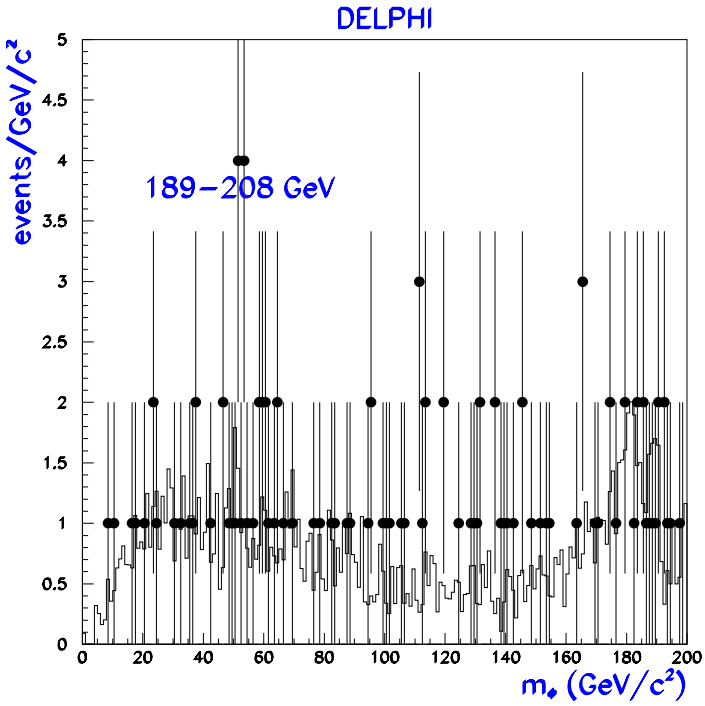

a)

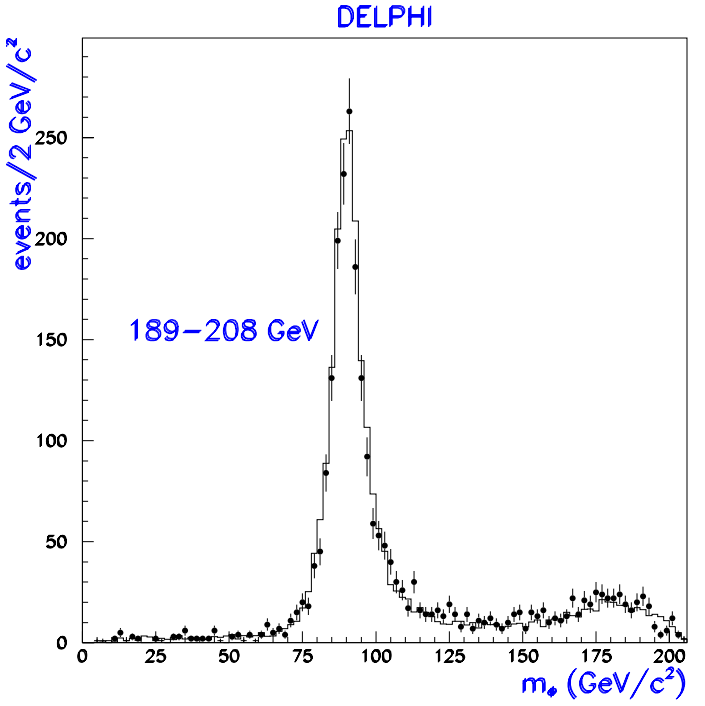

b)

Figure 8: a) Photon recoil mass spectrum for $\gamma\gamma\gamma$ candidates (points) and the expected background (histogram). The average number of entries per event in the data is 2.3. The bin size takes into account the experimental mass resolution and the expected signal width. b) Photon recoil mass spectrum for γgg candidates (points) and the expected background (histogram).

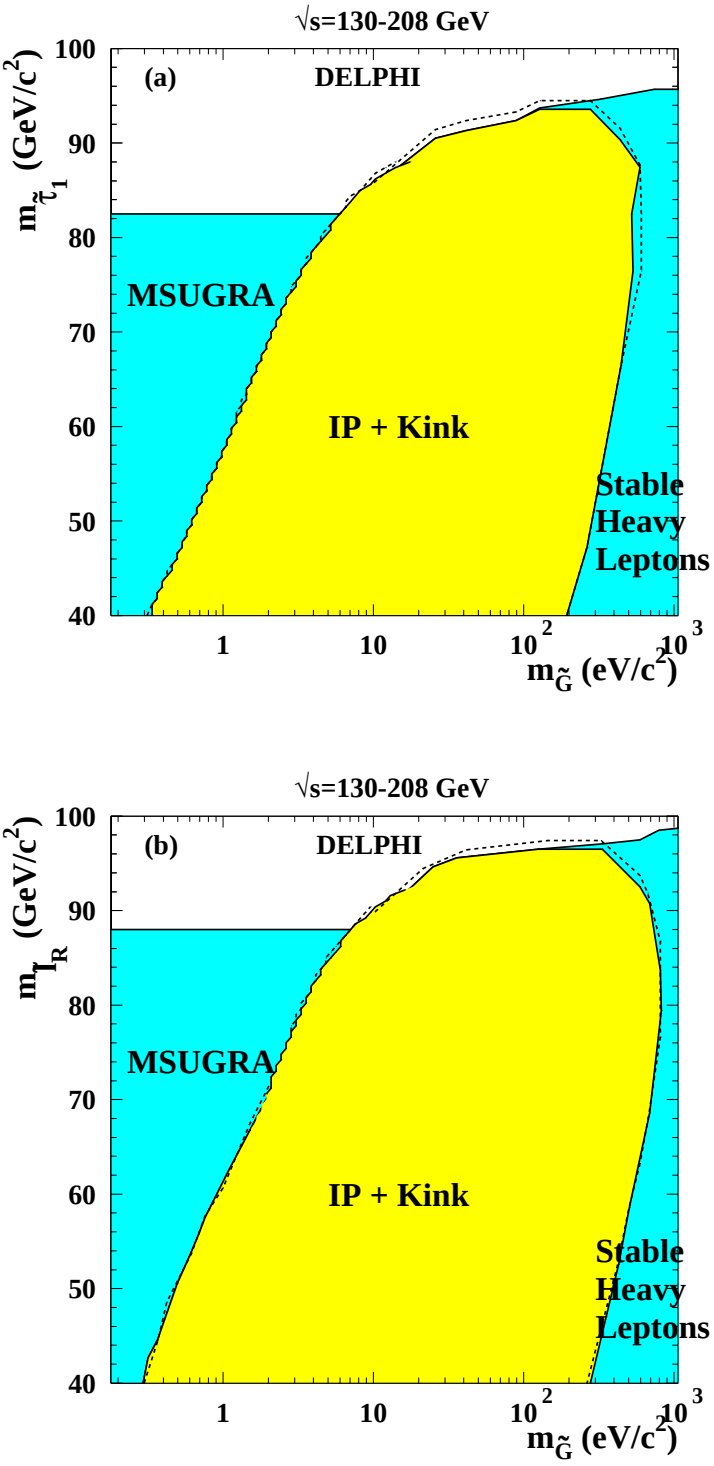

Figure 9: Exclusion regions in the ($m_{\tilde{G}}$,$m_{\tilde{\tau}_1}$) (a) and ($m_{\tilde{G}}$,$m_{\tilde{l}_R}$) (b) planes at 95% CL for the present analyses combined with the Stable Heavy Lepton search and the search for $\tilde{l}$ in gravity mediated models (MSUGRA), using all DELPHI data from 130 GeV to 208 GeV centre-of-mass energies. The dashed line shows the expected limits for the impact parameter and kink searches.

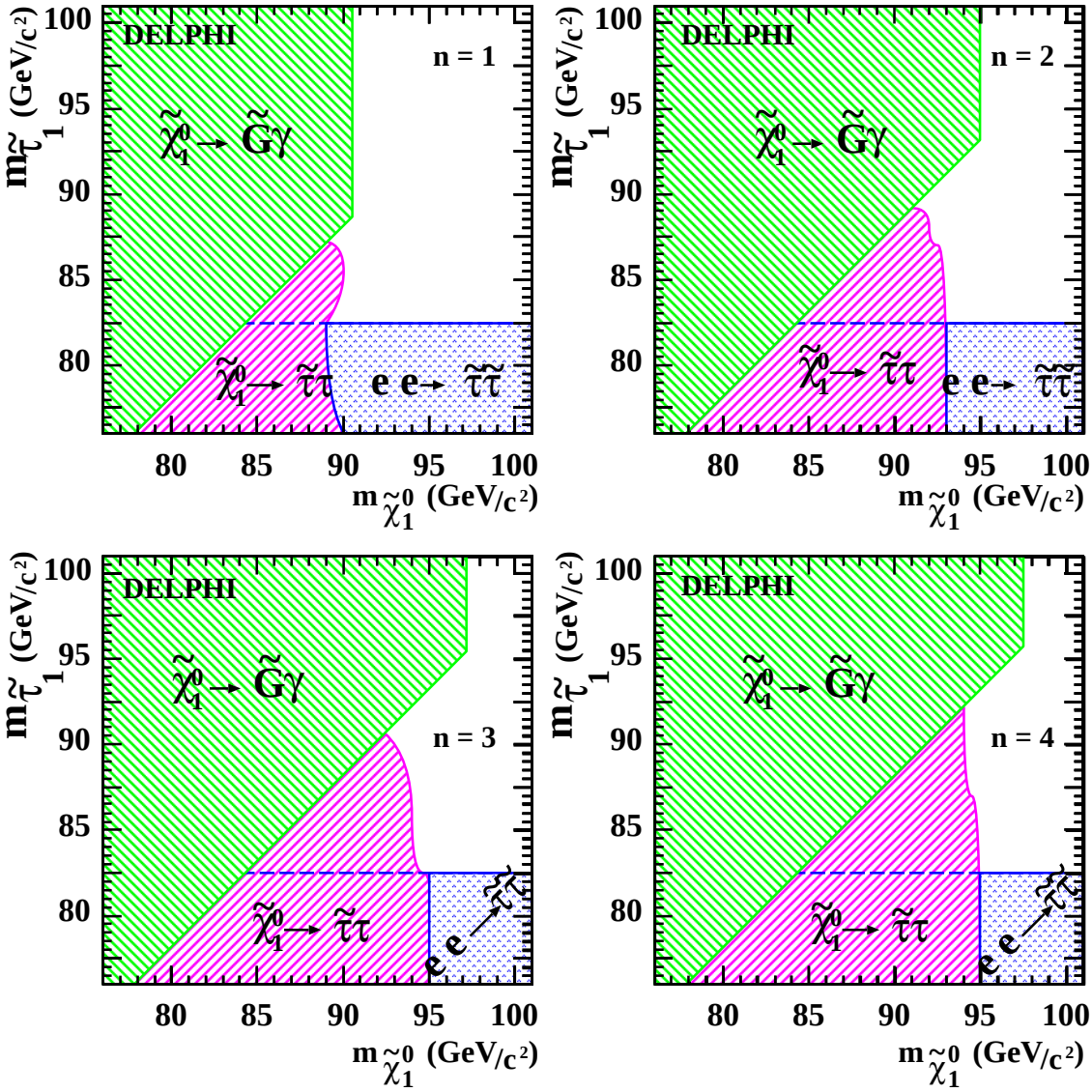

Figure 10: Exclusion regions in the ($m_{\tilde{\chi}_1^0}$,$m_{\tilde{\tau}_1}$) plane at 95% CL for the neutralino analysis (positive-slope dashed area) combined with the search for neutralino pair production followed by the decay $\tilde{\chi}_1^0 \to \tilde{G}\gamma$ (negative-slope dashed area), and the direct search for $\tilde{\tau}_1$ pair production within MSUGRA scenarios (point-hatched area), using all DELPHI data from 161 GeV to 208 GeV centre-of-mass energies.

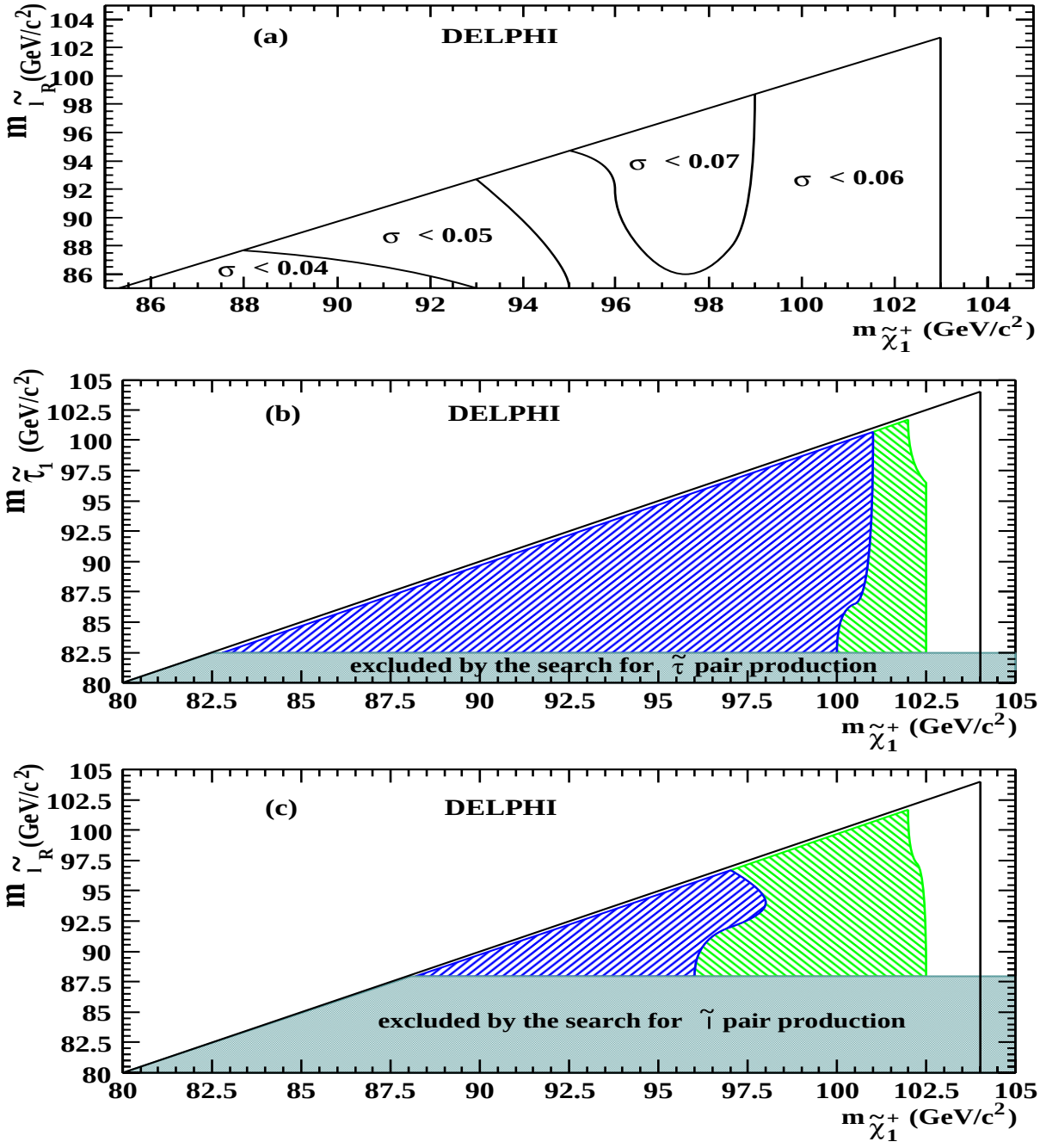

Figure 11: (a) Limits in picobarn on the lightest chargino pair production cross-section at 95% CL. Limits are shown as a function of $m_{\tilde{l}}$ and $m_{\tilde{\chi}_1^+}$ for $m_{\tilde{G}} = 100$ eV/c^2. Areas excluded at 95% CL in the ($m_{\tilde{\chi}_1^+}$,$m_{\tilde{\tau}_1}$) plane (b) and ($m_{\tilde{\chi}_1^+}$,$m_{\tilde{l}_R}$) plane (c). The positive-slope hatched area is excluded for all gravitino masses. The negative-slope hatched area is only excluded for $m_{\tilde{G}} > 100$ eV/c^2. The grey area is excluded by the search for stau pair production in gravity mediated supersymmetry breaking models. Both plots have been obtained using all DELPHI data from 183 GeV to 208 GeV centre-of-mass energies.

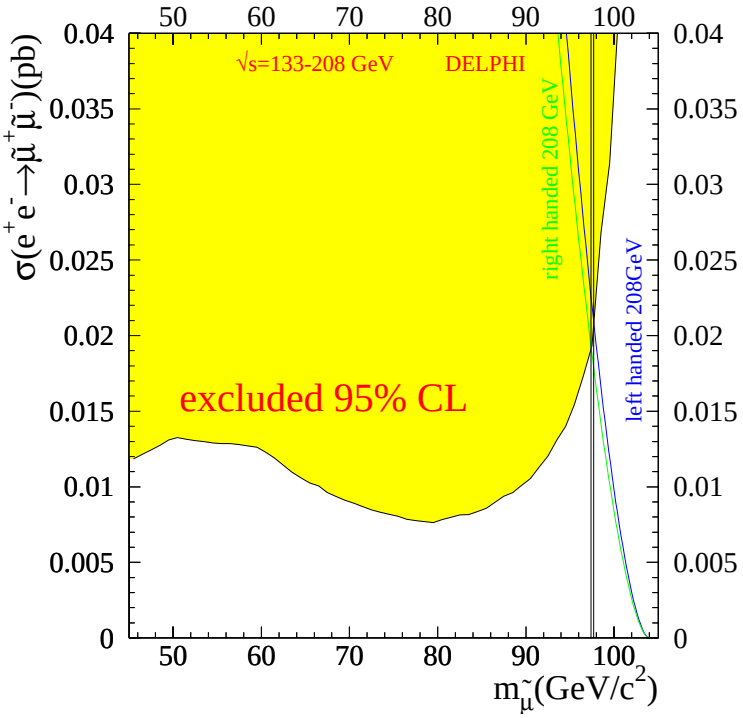

Figure 12: Predicted production cross-section for left and right handed stable smuons (staus) as a function of the particle mass. The cross-section limit indicated in the figure has been derived using all DELPHI data between 130 and 208 GeV.

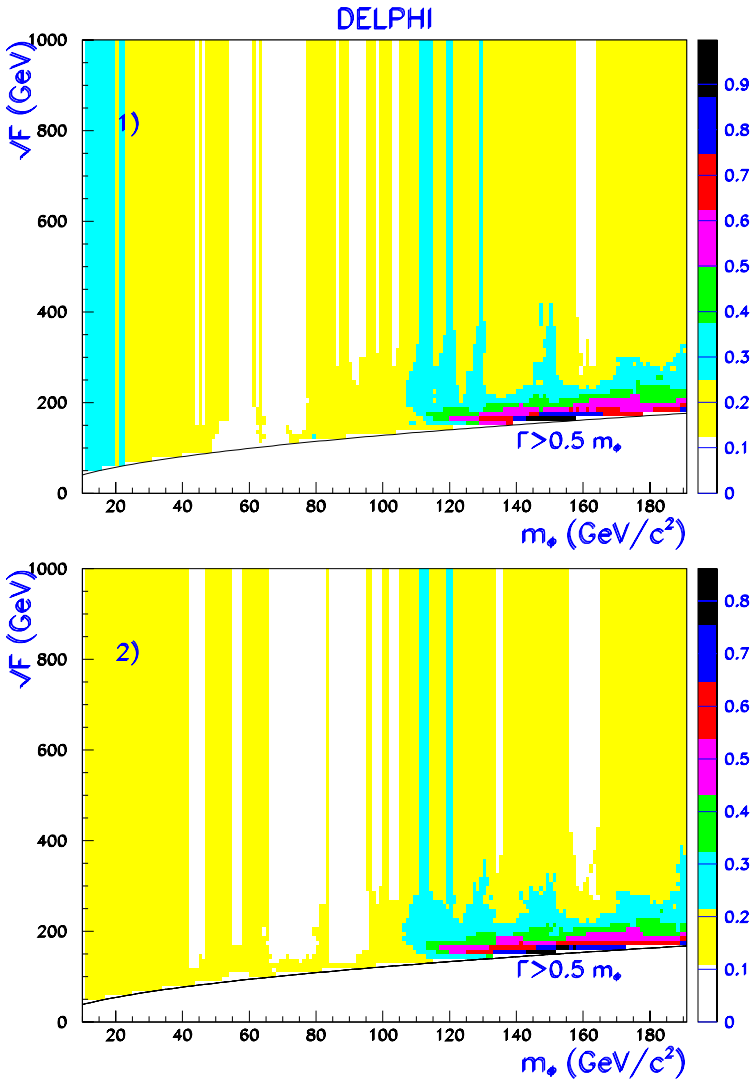

Figure 13: Cross section upper limit (pb scale on the right) at the 95% CL as a function of m_ϕ and $\sqrt{F}$ for the two sets of parameters of Table 1 and using all DELPHI data between 189 and 208 GeV.

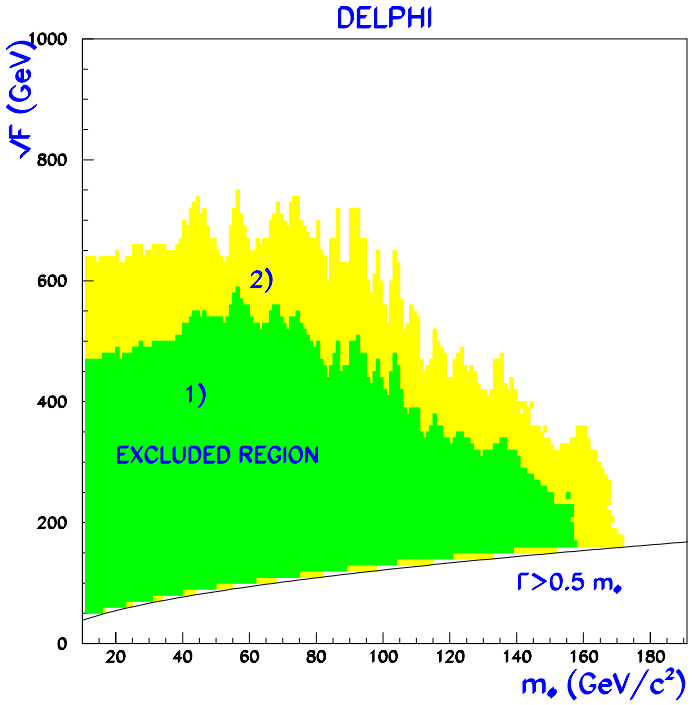

Figure 14: Exclusion region at the 95% CL in the $(m_\phi,\sqrt{F})$ plane using all DELPHI data between 189 and 208 GeV. Regions 1 and 2 are the excluded regions once the set of parameters (labelled with 1 and 2 respectively) of table 1 are applied.

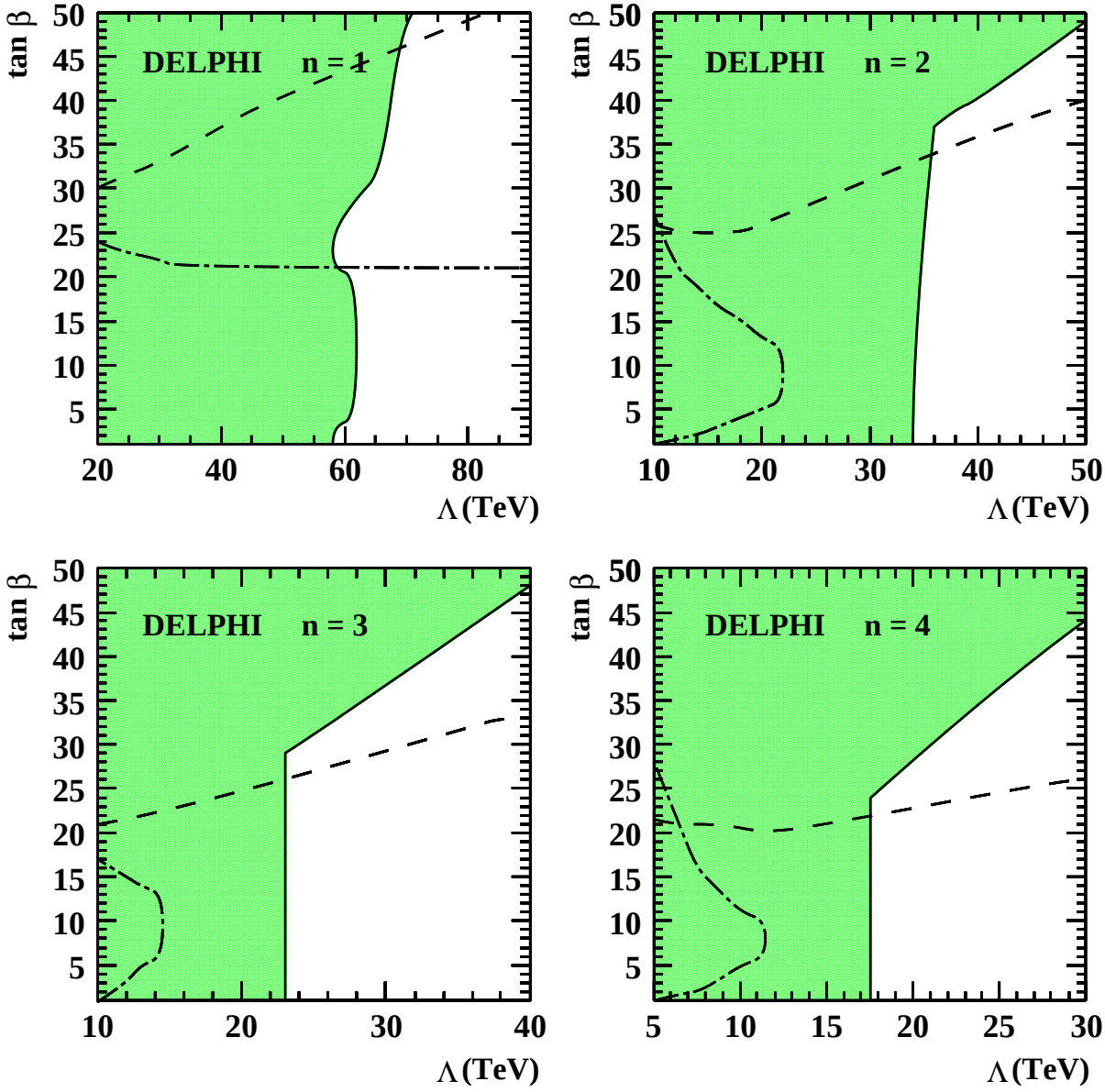

Figure 15: Shaded areas in the $(\tan\beta, \Lambda)$ plane are excluded at 95% CL. The areas below the dashed lines contain points of the GMSB parameter space with $\tilde{\chi}_1^0$ NLSP. The areas to the right (above for $n = 1$) of the dashed-dotted lines contain points of the GMSB parameter space were sleptons are the NLSP.